Arabian Journal of Chemistry (2022) **15**, 103784

King Saud University

Arabian Journal of Chemistry

www.ksu.edu.sa
www.sciencedirect.com

ORIGINAL ARTICLE

Ultrasound-assisted nanofluid flooding to enhance heavy oil recovery in a simulated porous media

Augustine Agi [a,b], Radzuan Junin [a,b,*], Mohd Zaidi Jaafar [a,b,*], Nor Aishah Saidina Amin [c], Mohd Akhmal Sidek [a,b], Bemgba Bevan Nyakuma [d], Faruk Yakasai [a,e], Afeez Gbadamosi [f], Jeffrey Oseh [g], Nur Bashirah Azli [a]

[a] *Department of Petroleum Engineering, School of Chemical and Energy Engineering, Faculty of Engineering, Universiti Teknologi Malaysia, 81310 Johor Bahru, Malaysia*
[b] *Institute for Oil and Gas (IFOG), Universiti Teknologi Malaysia, 81310 Johor Bahru, Malaysia*
[c] *Chemical Reaction Engineering Group (CREG), School of Chemical and Energy Engineering, Faculty of Engineering, Universiti Teknologi Malaysia, 81310 Johor Bahru, Johor, Malaysia*
[d] *Research Initiative for Sustainable Energy Technologies, Makurdi, Benue State, Nigeria*
[e] *Department of Chemical and Petroleum Engineering, Faculty of Engineering, Bayero University, Kano PMB 3011, Nigeria*
[f] *Department of Chemical and Petroleum Engineering, College of Engineering, Afe Babalola University, PMB 5454, Ado-Ekiti, Ekiti State, Nigeria*
[g] *Department of Petroleum Engineering, School of Engineering and Engineering Technology, Federal University of Technology, P.M.B. 1526 Owerri, Imo State, Nigeria*

Received 15 November 2021; accepted 8 February 2022
Available online 12 February 2022

KEYWORDS

Ultrasound;
Heavy oil viscosity;
Interfacial tension;
Silica nanoparticles;
Enhanced oil recovery;
Empty fruit bunch

Abstract Herein thermally treated empty fruit bunch SiO_2 nanoparticles (EFBSNP) was produced by ultrasound-assisted wet-milling and their effectiveness in enhancing cavitation effect of ultrasound to improve heavy oil recovery was evaluated. Empty fruit bunch ash (EFBA) was thermally treated to enhance its SiO_2 content. Surface properties and size distribution of EFBSNP were studied using transmission electron microscopy and dynamic light scattering. X-ray diffractometer identified the crystal phase, the active group was ascertain using Fourier-transform infrared spectroscopy and thermal stability was established by differential scanning calorimetry. Moreover, the surface chemical composition was determined by X-ray photoelectron spectroscopy. The ability of empty fruit bunch SiO_2 nanofluid (EFBSNF) to absorb ultrasound in heavy oil and the impact of ultrasound assisted EFBSNF flooding to enhance oil recovery of heavy oil was assessed. The microstructure analysis revealed EFBSNP of size ranges 17.78–115.38 nm with a purity of 94%.

* Corresponding authors at: Department of Petroleum Engineering, School of Chemical and Energy Engineering, Faculty of Engineering, Universiti Teknologi Malaysia, 81310 Johor Bahru, Malaysia.
E-mail addresses: r-radzuan@utm.my (R. Junin), mzaidi@utm.my (M.Z. Jaafar).
Peer review under responsibility of King Saud University.

Production and hosting by Elsevier

https://doi.org/10.1016/j.arabjc.2022.103784

EFBSNF assisted ultrasound decreased interfacial tension to 0.2 mN/m, thus mobilizing the trapped oil droplet in the pores effectively. Ultrasound assisted EFBSNF flooding increased oil recovery by 44.33% compared to 26.33% without ultrasound.

Nomenclature

ASTM	American society for testing and material
CFNS	Copper ferrite nanoparticles
DLS	Dynamic light scattering
DSC	Differential scanning calorimetry
EDXRF	Energy dispersion X-ray fluorescence
EFB	Empty fruit bunch
EFBA	Empty fruit bunch ash
EFBSNF	Empty fruit bunch silica nanofluid
EFBSNP	Empty fruit bunch silica nanoparticles
EOR	Enhanced oil recovery
FTIR	Fourier-transform infrared spectroscopy
GMS	Gatan microscopy suite
HRTEM	High-resolution transmission electron microscope
ICDD	International centre for diffraction data
IFT	Interfacial tension
OOIP	Original oil in place
O/W	Oil-water
TEM	Transmission electron microscope
Tg	Glass transition
XPS	X-ray photoelectron spectroscopy
XRD	X-ray diffractometer
XRF	X-ray fluorescence

1. Introduction

Rising global energy demand has led the oil and gas industry to develop unconventional sources of heavy oil to meet energy needs. Unlike conventional (light) oil, heavy oil is difficult to extract and transport because it has low mobility due to high viscosity, high carbon to hydrogen, high asphaltene and resin content (Gbadamosi et al., 2019a). To date, oil recovery from heavy oil reservoirs has been achieved by thermal recovery techniques such as combustion, steam-assisted gravity drainage, steam and hot water injection. However, the application of these techniques to thin and deep reservoir formations results in low oil recovery due to the high heat loss to overburden layers (Saboorian-Jooybari et al., 2016). Moreover, the high energy requirement for these methods increases the operating cost and environmental impact. For instance, about 10% of the water produced during heavy oil extraction are disposed and it contains varieties of heavy metal pollutants which may contaminate clean groundwater, or harm plant and animal life. Also, emission of CO_2 for heavy oil development and processing is about 110 kg per barrel which is three times higher than the amount required for a barrel of crude oil (Marrow et al., 2014). Therefore, alternative methods have been sought to enhance recovery of heavy oil.

Ultrasound is an unconventional method that aims to transfer energy to affect the physical and chemical properties of heavy oil (Hamidi et al., 2017). Ultrasound creates cavitation bubbles that generate high energy and pressure upon collapse to upgrade heavy oil by breaking down large molecules (Montes et al., 2018). However, the increased resistance due to the shielding layer of asphaltenes and colloids in heavy oil increases the cavitation threshold (Huang et al., 2018). Therefore, the effect of cavitation by ultrasound should be greater which is not always the case resulting in a lower cavitation effect. Nanoparticles are known to enhance the cavitation effect by generating free radicals for hydrogenation and cracking reactions. Consequently, they absorb asphaltenes and act as a catalyst to break down the structure of the heavy oil (Huang et al., 2018). So far, the focus has been on metal oxide nanoparticles such as iron oxide, magnesium, titanium, zinc oxide and copper oxide (Mateus et al., 2021) but environmental concerns regarding the use of these metal nanoparticles and cost of producing them have hindered their industrial application (Agi et al., 2020a).

The successful application of silica (SiO_2) nanoparticles in enhanced oil recovery (EOR) to improve the rheology of displacing fluid (Gbadamosi et al., 2019a; Kumar et al., 2022), as nanocomposite (Kazemzadeh et al., 2018; Ali et al., 2021a), in stabilizing foam (Rezvani et al., 2020) and improve EOR mechanisms of surfactants (Asl et al., 2020) has necessitated interest in the production of (SiO_2 nanoparticles from renewable sources such as sugarcane straw (Rovani et al., 2018), rice husks (Agi et al., 2020b), palm kernel shells (Imosili et al., 2020) (Table 1). The choice of renewable sources as the basic raw materials to produce SiO_2 nanoparticles is owing to their broad material source, high hydrophobicity, catalytic support, low cost and environmental friendliness (Kenes et al., 2012; Imoisili et al., 2020). Chemical treatment has been used to produce SiO_2 nanoparticles, but this process requires chemicals that are not environmentally friendly, the process can be expensive, and the presence of impurities affects the productivity of SiO_2 nanoparticles (Pineda-Vasquez et al., 2014; Fernandes et al., 2017). Therefore, the synthesis method and the removal of impurities before reaction, is one of the obstacles in the production of SiO_2 nanoparticles (Fernandes et al., 2017).

Wet milling is a physical synthesis method used to design material for a specific application. These can be achieved by assigning the product with a specific area and porosity during the milling process. The advantage of this method is that it can minimize waste by producing nanoparticles that are easy to handle and can improve properties of the nanoparticle for better flowability (Lee, 2013). However, poor wetting during milling causes component segregation and broad particle size distribution (Lee, 2013). Ultrasonication treatment is a process intensification method used for redispersion, facilitating mixing, chemical reaction, surface interaction, heat and mass transfer to produce particles with small size range (Agi et al., 2019a, 2020a, 2021). Process intensification of synthesis and treatment methods can enhance the properties of nanoparticles for industrial applications (Kenes et al., 2012; Agi et al., 2019a; Agi et al., 2020b). Albeit Agi et al. (2020b) produced SiO_2 nanoparticles from rice husk using a physical method, the process was not intensified. Similarly, Fernandes et al. (2017) thermally treated SiO_2 to improve the purity, but their study was limited to microparticles only. Notwithstanding, Montes et al. (2018) reduced the viscosity of heavy oil by catalytic decomposition of heavy fraction by ultrasonic cavitation using metal oxide nanoparticles. Their studies were limited to the functionalization of the nanoparticles and viscosity

Table 1 Summary of published literature on application of SiO_2 in EOR.

Author Year	Porous Media	Application	Oil Recovery
Montes et al. (2018)	Not Stated	SiO_2 was used as catalyst to decrease viscosity of heavy oil using ultrasound	Not Stated
Kazemzadeh et al. (2018)	Carbonate Sand pack	Nanocomposite	Incremental oil recovery of 14–24%
Gbadamosi et al. (2019)	Sandstone Core	SiO_2 nanoparticles was used to improve the rheological properties of HPAM	63.2% OOIP
Asl et al. (2020)	Carbonate Cores	SiO_2 nanoparticles was used improve EOR mechanisms of surfactants.	56.9% OOIP
Rezvani et al. (2020)	Glass Micromodel	SiO_2 nanoparticles was used to stabilize foam	92% OOIP
Agi et al. (2020)	Sandstone Core	SiO2 was used to improve the thermal degradation of HPAM	24% Incremental oil recovery
Ali et al. (2021a)	Carbonate Core	Nanocomposite	46.53% OOIP
Ali et al. (2021b)	Carbonate Core	Nanocomposite	Not Stated
Kumar et al. (2022)	SiO_2 Plate	SiO_2 was used to improve the rheological properties of HPAM	Not Stated

reduction. In similitude, Mateus et al. (2021) synthesised magnetic copper ferrite nanoparticles (CFNS) for heavy oil viscosity reduction. The rheological evaluation showed a viscosity reduction of 18% with CFNS influenced by the decrease in elastic and viscous moduli of the heavy oil. Nevertheless, the focus of previous studies has been on viscosity reduction whereas other EOR mechanisms were not considered. Likewise, the oil displacement efficiency of the combined method of nanofluid and ultrasound was not investigated. Therefore, ultrasound-assisted wet milling method is a novel process intensification method. Also, ultrasound-assisted flooding using nanofluids to improve EOR has not been reported in literature. Furthermore, the mechanisms of ultrasound assisted nanofluid flooding has not been explained in any literature.

Herein thermally treated empty fruit bunch SiO_2 nanoparticles (EFBSNP) was produced by ultrasound-assisted wet-milling and their effectiveness in enhancing cavitation effect of ultrasound to improve heavy oil recovery was evaluated. Moreover, empty fruit bunch ash (EFBA) was thermally treated to increase its SiO_2 content and the chemical components were investigated by X-ray fluorescence (XRF). Similarly, the surface properties and size distribution of EFBSNP were investigated by transmission electron microscope (TEM) and dynamic light scattering (DLS). In addition, an X-ray diffractometer (XRD) was used to identify the crystal phase, whereas the active group was ascertain using Fourier-transform infrared spectroscopy (FTIR) and differential scanning calorimetry (DSC) was used to determine the thermal stability. Moreover, the surface chemical composition was determined by X-ray photoelectron spectroscopy (XPS). The ability of empty fruit bunch silica nanofluid (EFBSNF) to absorb ultrasound in heavy oil was investigated. Finally, the effect of ultrasound assisted EFBSNF flooding was evaluated and the possible oil recovery mechanisms were revealed.

2. Materials and methods

2.1. Materials

Empty fruit bunch (EFB) fibres were obtained from Felda Palm Oil Mill, Kulai, Johor, Malaysia. Ethanol (biological grade with a molecular weight of 46.07 g/mol), with a purity of 99.8% (v/v) was purchased from R & M Chemicals. Sodium chloride (NaCl, molecular weight 58.44 g/mol) with a purity of 99.8% assay was obtained from QReC^{TM}. Heavy mineral oil with a viscosity of 240 mPa.s and density (0.92 g/cm^3) was obtained from Merck KGaA, Germany. Unconsolidated sandpack was used as the porous media (Table 2).

2.2. Methods

2.2.1. Thermal treatment

EFB was washed with distilled water to remove dirt and sun-dried to reduce moisture then burned to obtain ash. The dried EFBA was thermally treated at 1100 °C in a chamber furnace (Carbolite Gero 300) for 4 h and allowed to cool in the furnace. The thermal treatment was used to remove impurities and carbonaceous materials present in the EFBA and to increase the SiO_2 content of the EFBA (Fernandes et al., 2017; Agi et al., 2020b). This temperature range was chosen because crystallization of SiO_2 occurs above 800 °C (Agi et al., 2020b) and above 1100 °C no significant change occurred.

2.2.2. Formulation of EFBSNP

About 40 g of the thermally treated EFBA was placed in a grinding jar made of tungsten carbide, thereafter, round balls made of tungsten carbide was used to fill the grinding jar up to 150 mL. The grinding jar (holder) was placed eccentrically in a Retsch PM 100 planetary ball mill equipment (Fig. 1a). Dry milling of EFBA was initiated for 20 min (rotating-reversing motion) at 10 min intervals for 2 h. Subsequently, 10 mL of ethanol was added to the EFBA to act as a control agent of the process (Wang et al., 2017; Zhang et al., 2018; Agi et al., 2020b). This time the ball speed (500 rpm) and the grinding jar created an interaction (frictional forces) releasing high energy to the EFBA for 4 h (Fig. 1b). Consequently, the exchange of these forces resulted in comminution. The sample was then washed with ethanol and placed in an ultrasonic bath (Genesis™ XG-500-6, 40 kHz, 500 W) for 1 h. Thereafter, the sample was centrifuged and dried in an oven for 24 h. Fig. 2 shows the schematic illustration of the formulation process.

2.2.3. Morphological analysis

The shape and size in micrometre of the EFBA was studied using Hitachi S-3400N scanning electron microscopy (SEM) with a back-scattering electron detection. The sample was placed on a metal tub and sputtered with gold to make it conductive before observation. The image was captured at an accelerating voltage of 10 kV. The equipment has an inbuilt

Table 2 Properties of porous media used for the heavy oil displacement experiments.

Sand pack	Fluid Type	Length (cm)	Diameter (cm)	Pore Volume (cm^3)	Bulk Volume (cm^3)	Porosity (%)	Permeability (D)
P1	Water	25	4	103	236	44	3.7
P2	EFBSNF	25	4	102	236	43	3.3
P3	EFBSNF + Ultrasound	25	4	98	236	42	3.1
P4	EFBSNF (0.05 wt%)	25	4	101	236	43	3.6
P5	EFBSNF (0.1 wt%)	25	4	97	236	41	3.4
P6	EFBSNF (0.2 wt)	25	4	95	236	40	3.0

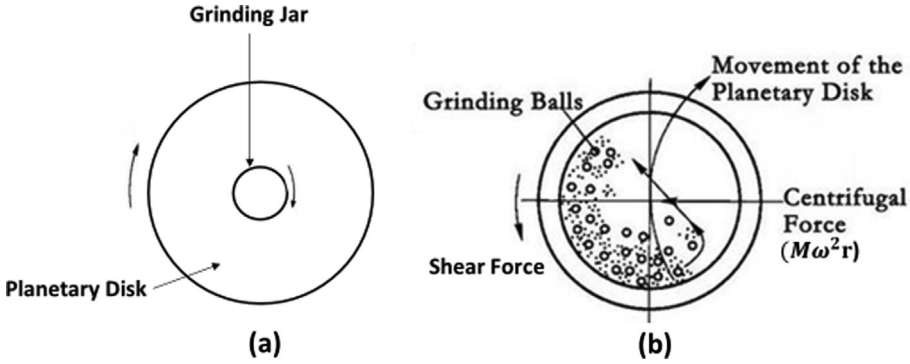

Fig. 1 Schematic illustration of the working principle of planetary ball mill showing (a) general layout of the disk with the arrows indicating the counter-rotation of the supporting disc and (b) horizontal cross-section of grinding jar with the arrows indicating the counter-rotation of the milling beaker.

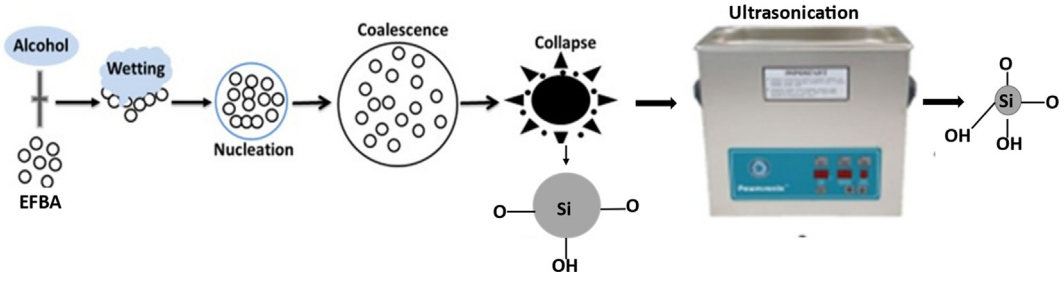

Fig. 2 Schematic illustration of EFBSNP formulation process.

HITACHI EMIP-SP electron microscope image integration software to automatically measured and enhanced the images of the particles. A high-resolution TEM (HRTEM, JEOL, JEM-ARM200F) was used to determine size (in nanometre) and shape of the EFBSNP. The sample was prepared by dispersing in water and placed on a graphene-coated substrate. Detection was achieved at an accelerating voltage of 200 kV. A Gatan microscopy suite (GMS3) software was used to automatically analyse the TEM images and the particles sizes determined.

2.2.4. Chemical composition analysis

The elemental composition of EFBA was compared by energy dispersion X-ray fluorescence (EDXRF, Rigaku NEX CG Japan). It was operated under helium at 0.6 L/min and the weight percentages in the form of oxides were determined.

2.2.5. Particle size distribution measurement and stability determination

The size distribution of EFBA was measured using Malvern Mastersizer 300 (Malvern Instrument Ltd, Worcestershire, UK). The instrument utilizes laser diffraction to calculate the size distribution in volume precent using Mastersizer 300 software (v.5.54). The size distribution of EFBSNP, and the zeta potential of EFBA and EFBSNP were determined using the apparatus Malvern Zetasizer Nano ZSP, UK. The instrument utilizes dynamic image analysis to calculate particle size in number percent. For this purpose, (0.05, 0.1 and 0.2 wt%) of

EFBA and EFBSNP were dispersed in distilled water with a refractive index of 1.330 and viscosity of 0.8872 mPa.s. The solution was sonicated for 30 min to obtain a homogenous solution and kept for 24 h. Thereafter, the samples were transferred to omega cuvette for analysis. The measurements were conducted at a back-scattering angle of 170 °C at 22.5 °C (room temperature). The zeta potential was determined by measuring the particle velocity in electrical field. The measurement was performed at 22.5 °C using Zetasizer™ software (v.7.03).

2.2.6. Crystalline structure

The crystalline structure of EFBA and EFBSNP were determined using XRD (Rigaku SmartLab, Japan). The device was operated at 40 kV, 30 mA with a Cu-Kβ irradiation. The scanning angle of diffraction (2θ) ranged from 3 to 100° at a scanning speed of 8.2551 deg/min. This scanning range was chosen based on literature (Onaja et al., 2017; Jie et al., 2019).

2.2.7. Chemical structure

The functional groups of EFBA and EFBSNP were detected by FTIR (Frontier, PerkinElmer). The samples were mixed with potassium bromide and compressed under high pressure to form a pellet. The pellet was used for FTIR measurement at room temperature in the range of 650–4000 cm^{-1}.

2.2.8. Thermal properties

The thermal stability properties of EFBA and EFBSNP were investigated using Mettler-Toledo DSC 1. The ice machine refrigeration system and STARe software were used for the analysis. The temperature of the heat flow was calibrated using indium and zinc as standards. The measurement was done at 30–500 °C (this temperature range above 0 °C was chosen to depict high temperature reservoir condition), at a heating rate of 10 °C/min with nitrogen as the purge gas. The melting point was determined as the beginning of the peak and the midpoint of the heat capacity as the glass transition temperature (ASTM E2161-08).

2.2.9. Surface chemical composition

The surface chemical composition of EFBA and EFBSNP were determined by XPS (Axis-Ultra DLD Shimadzu). The instrument was equipped with monochromatic Al Kα as the exciting source. The spectra were calibrated using standard binding energy value of carbon (284.6 eV) as reference.

2.2.10. EFBSNF and brine preparation

To produce EFBSNF, different concentrations of EFBSNP (0.05–0.2 wt%) were dispersed in deionized water and stirred using a magnetic for 1 h. This concentration was chosen based on literature (Maghzi et al., 2013; Gbadamosi et al., 2019b; Agi et al., 2020b). Subsequently, the solution was ultrasonicated for 30 min to form a stable and homogenous solution. The brine solution was prepared by dispersing 2.2 wt% of NaCl in deionized water and the mixture was stirred for 1 h.

2.2.11. Ultrasonic absorption efficiency of EFBSNF

In this study, 100 mL of deionized water was ultrasonicated and the temperature was measured every 30 s. using a thermometer. Then, different concentrations of EFBSNF (0.05–0.2 wt%) and 0.2 wt% of EFBA were ultrasonicated and the temperature was determined. Also, different concentrations of EFBSNF (0.05–0.2 wt%) and EFBA (0.2 wt) were dispersed in 100 mL of heavy oil sample as described elsewhere (Montes et al., 2018). The sample was ultrasonicated and the temperature determined every 30 s for 2 min 30 s.

2.2.12. Heavy-oil viscosity reduction ability of EFBSNF

The viscosity of the heavy oil sample was determined with time using digital viscometer Anton Par SVM 3000. Then, the viscosity of the sonicated heavy oil with (0.05–0.2 wt%) and without EFBSNF was determined at 30 s interval of ultrasound. EFBSNF was used as a catalyst to produce free radicals for hydrogenation and cracking of the heavy oil. For this purpose, 2.5 mL of the heavy oil sample was injected into a hose pipe using a syringe. The hose delivered the oil sample to the measurement chamber where the viscosity was measured and recorded. After each test, the equipment was cleaned with toluene to remove impurities and sample debris.

2.2.13. Oil displacement experiments

The experimental setup for the oil displacement experiments consists of a cylindrical sand pack made with a polyvinyl chloride containing sandstone of size range 125–250 μm. The sand pack was used as a porous medium to investigate the oil displacement ability of EFBSNF under ultrasound (Table 2). The joints of the sand pack were sealed with adhesives to prevent any leakage during the experimental process. Sieves placed at both ends of the cylinders prevented fines migration. Thereafter, the properties of the porous media were determined (Table 2). Then the sand pack was placed in a holder and immersed in the ultrasonic bath to achieve maximum ultrasonic exposure (Fig. 3). The ultrasonic generator (Gene-

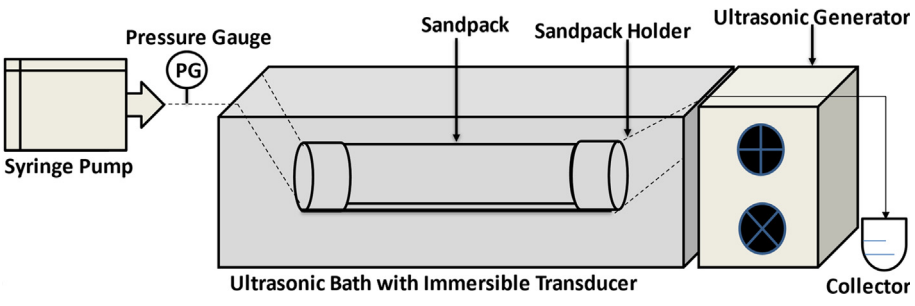

Fig. 3 Schematic illustration of ultrasound assisted EFBSNF flooding in a simulated porous media.

sis™ XG-500–6, 500 W) delivered high frequency (40 kHz) waves through the water-bath with the immersion transducer. This frequency was chosen based on the application as high frequency increases the number of free radicals (electron transfer) (Thompson and Doraiswamy, 1999). Subsequently, 2.2 wt % NaCl (brine) was introduced into the sand pack with aid of a syringe pump (NE-1000) until it was completely flooded (saturated). Heavy oil was introduced at 2.0 mL/h until connate water saturation was achieved. Thereafter, the water saturation and oil saturation were determined. The sand pack was then flooded with water until breakthrough occurred. In this study EFBSNF flooding and ultrasound assisted EFBSNF were considered as EOR process. Hence to extract the bypassed oil, 0.5 PV of 0.05–0.2 wt% EFBSNF was injected and then ultrasound wave was used for 15 min to assist EFBSNF flooding. Ultrasound was applied under uncontrolled temperature and the temperature of the system increase to 65 °C. To extract any left-over oil 0.5 PV of chase water was injected into the system. The experiments were repeated twice and the average reported.

3. Results and discussion

3.1. Thermally treated EFBA

The chemical composition of EFBA before and after thermal treatment was determined by XRF (Table 3). The EFBA before treatment showed 60% SiO_2 and trace-elements such as magnesium oxide (MgO), aluminium oxide (Al_2O_3), phosphorus pentoxide (P_2O_5), potassium oxide (K_2O), calcium oxide (CaO), titanium oxide (TiO_2), and iron (iii) oxide (Fe_2O_3). Thermal treatment was used to improve the SiO_2 content to serve as an alternative source of SiO_2. The XRF results (Table 3) show a significant decrease in the concentration of the trace element with increasing temperature and a corresponding increase in SiO_2 content. This is because when phase transition occurs (when temperature exceed 573 °C), SiO_2 crystal lattice structure changes. Heating will cause the impurities to be mobile and diffuse from the inclusion to the crystal lattice under thermodynamic driving force. However, diffusion during the phase transition is accelerated by thermodynamic forces because SiO_2 has a loose structure, therefore some of the impurities enter the SiO_2 crystal lattice thereby increasing the SiO_2 phase (Jani and Hogland, 2017; Li et al., 2020). This result is consistent with previous study of Kenes et al. (2012), they reported that higher temperature causes thermal decomposition of organic substance in rice husk and hence the SiO_2 content increases.

Table 3 XRF analysis of untreated and treated EFBA.

Component	EFBA (%)	Treated EFBSNP (1100 °C) (%)
SiO_2	60.3 ± 0.127	94.46 ± 0.002
Na_2O	ND	ND
MgO	3.04 ± 0.108	ND
Al_2O_3	4.03 ± 0.0259	ND
P_2O_5	2.38 ± 0.0083	ND
K_2O	10.9 ± 0.0330	1.48 ± 0.0201
CaO	8.22 ± 0.0286	1.33 ± 0.001
TiO_2	0.347 ± 0.004	ND
MnO	0.165 ± 0.0024	ND
Fe_2O_3	10.6 ± 0.0174	2.73 ± 0.001

ND: Not detected.

3.2. Morphology results

The SEM image of untreated EFBA (Fig. 4a) shows spherical, angular and irregular shapes. The treated EFBA showed a decrease in spherical shape with temperature (Fig. 4b), which can be attributed to the collapse of some micro and mesopores at high temperature (Liu et al., 2013). The particle size also increased with temperature (Fig. 4b). At high temperature, crystal growth is enhanced, which promotes the emergence of a more compact structure. Similar result was reported by Chen et al. (2012) when they stated that particle structure becomes more packed when the temperature exceeds 600 °C. The result agrees with previous studies by Fernandes et al. (2017) who found that high temperature decreases the specific surface area values and thus increases the diameter of the particles. TEM was used to confirm the shape and size of EFBSNP (Fig. 5). The size of EFBSNP ranges from 17.78−115.38 nm. The larger particles have a platy and irregular shape (Fig. 5a), while the smaller particles have a spherical shape (Fig. 5b). The irregular shape could be due to cavitation during wet milling. During shearing of ethanol during the wet milling, the wetted particles forms nucleus resulting in nucleation of individual particles coated with a layer of liquid, low pressure produces liquid bubbles (Fig. 2), the subsequent growth and collapse of these bubbles produces cavitation effect which improves the particle size reduction efficiency of the ball mill (Sen, 2017; Agi et al., 2020b). Subsequent ultrasonic treatment of EFBSNP changed the shape of the particles from irregular and angular to spherical (Ahmad et al., 2020). This confirms that the change in size and shape during the thermal treatment of EFBA had no effect on the resultant EFBSNP after wet milling but rather it increased the surface stability (Reynolds et al., 2016).

3.3. Mechanisms of EFBSNP synthesis via ultrasonic-assisted wet milling

During the process of dry milling, a mild compacting force was propagated to produce a mixture of fine micro particles. The alcohol inhibited the aggregation of the samples during wet grinding. Therefore, the alcohol adsorbed the particles by shielding the attractive force while promoting steric stabilization. Nevertheless, the adsorption of alcohol prevented agglomeration through the mechanism of electrostatic stabilization (Loh et al., 2015). Then the mechanical energy of the mill (impact of mill ball) exerts a tension on the particles, which leads to nucleation (first step in the formation of a new phase). A high rotational speed of the ball mill (500 rpm) increases the collision between the particles or between the particle and the wall and increases the energy transfer to the particles leading to coalescence (Fig. 2). In addition, the revolution of the ball mill might have increased the temperature forcing the internal liquid and air out and forming liquid film on the surface. This process accelerates the size increase and growth of the particles (Wang et al., 2017). The final stage in the mechanism of wet milling is the breakage

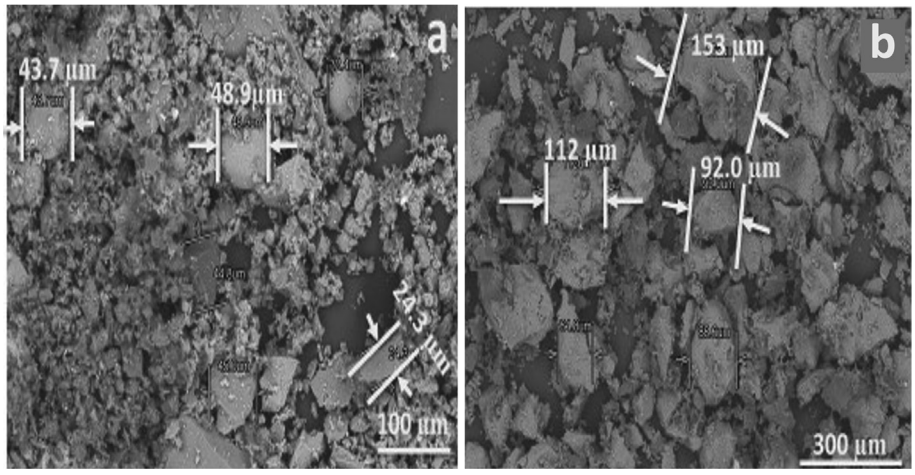

Fig. 4 SEM images of EFBA showing shapes and sizes (a) untreated having spherical, angular and spherical shapes with small particle sizes and (b) treated at 1100 °C having larger particle sizes.

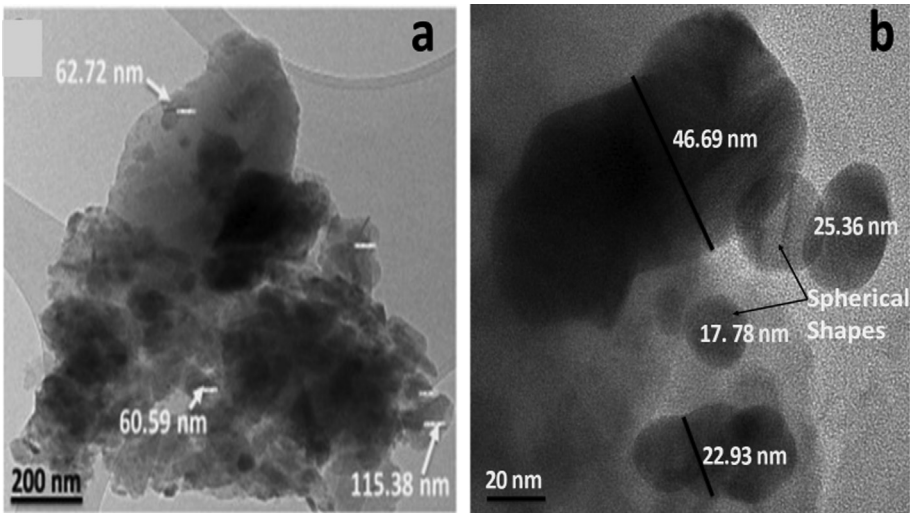

Fig. 5 TEM images of EFBSNP showing sizes and shape (a) platy and irregular shapes due to cavitation during wet milling and (b) spherical shape and small size particles due to ultrasonication.

and attrition, which is initiated by the shear force of the ball mill. This occurs when the applied kinetic energy exceeds the energy the granules can resist (Agi et al., 2020b). After wet milling, some EFBSNP was assumed to remain in the aggregates (Fig. 5a). Therefore, ultrasonic treatment was used to dissociate the EFBSNP in the aggregates to form radicals which may have induced the degradation/detexturation and sono-erosion of EFBSNP altering the morphology (Fig. 5b).

3.4. Size distribution and surface charge of EFBSNP

The size distribution of EFBSNP reduced to nanosize by wet milling and ultrasonic treatment compared to the micron size of the untreated (supplementary information Fig. S1-2). EFBA (Figure S1) showed a broad size distribution consistent with the different sizes and shapes of the SEM result (Fig. 4). In contrast, EFBSNP (Figure S2) exhibited a narrow size distribution, which could be attributed to the effect of ultrasonic homogenization that controlled the particle size, resulting in a narrow size distribution (Gokce et al., 2014). Zeta potential was used to determine the stability of EFBSNP in solution. As a reference, zeta potential values within ±10 mV, ±10–20 mV, ±20–30 mV and ±30 mV suggest very unstable, reasonably stable, moderately stable, and highly stable nanofluids, respectively (Chakraborty and Panigrahi, 2020). Fig. S3-4 show the zeta potential and surface charge of EFBA and EFBSNP. The surface chemistry imparts stability to the colloids, which greatly influence the flow behaviour of nanosuspension. Therefore, the zeta potential can affect the stability of solutions. This is because the electrostatic repulsion between particles is greater at high zeta potential. Figure S4 shows that the zeta potential of EFBSNP can be affected by thermal treatment. This is because above 600 °C, the ratio of inaccessible silanol group to associated silanol increases, which may have increased the surface charge of EFBSNP (Tettey and Lee, 2013). Consequently, EFBSNP zeta potential at different con-

centration lies between −36.7 and 38 mV which is higher compared to EFBA at different concentration (−26.1 to 28.8 mV) (Figures S3 and 4). This implies that pH has a direct effect on zeta potential since the electrostatic forces were retained by the pH during wet grinding. In the preparation of nanoparticles during wet milling, pH is a vital parameter (Sakthivel et al., 2007). Kaya and Yukselen (2005) recommended a pH of 7.2 for quartz materials. Therefore, the pH of 7.3 for the alcohol used might have limited deposition of EFBSNP and maintained the electrostatic and steric stabilization of the crystals in EFBSNP to produce a very stable nanoparticle through wet milling. Nevertheless, the constant pH of the medium implies that the ultrasound had no significant effect on the zeta potential (Jafari et al., 2014). Also, the particle size distribution, zeta potential of EFBA and EFBSNP at different concentration showed significant similarity this implies that the change in concentration had no significant impact on the size distribution and zeta potential.

3.5. Crystalline structure of EFBSNP

The XRD results of EFBA show the presence of amorphous and crystalline phases (Fig. 6a). Two crystal phases of SiO_2 (quartz and tridymite) were identified. Quartz was identified as the major crystalline phase with at sharp peak of 2θ at 26.57° and at 20.8°, 50.08° and 59.8°. These peaks correspond to the reflection from 011, 110, 112 and 121. Also, tridymite crystalline phase of 2θ at 21.8°, 28.3°, 31.1° and 36.4° corresponds to 101, 111, 102 and 200 crystal planes of alpha-SiO_2. These results matched with the standard given in the international centre of diffraction data (ICDD) 01-077-1060. This implies that the crystal plane of the SiO_2 is hexagonal with a lattice parameter of a-axis (4.9 Å), b-axis (4.9 Å) and c-axis (5.4 Å). This indicates that the EFBA has both quartz and tridymite peaks. Similar result was reported by previous studies of Fernandes et al. (2017); Borouni et al. (2018) and Imoisili et al. (2020). Subsequently, the thermal treatment affected the crystalline phase of the EFBSNP (Fig. 6a). This is because high temperature assists the formation of the crystalline phase due to the energy added to the system (Fernandes et al., 2017). For example, crystallization of quartz occurred between 573 and 1055 °C, while tridymite crystallized at 867 °C (Fernandes et al., 2017; Borouni et al., 2018). Consequently, the crystallization rate increased from 10% (EFBA) to 46.78% (EFBSNP). This could be due to a diffusion-induced mechanism during the wet milling that may have influenced the kinetic transformation to a more crystalline phase (Agi et al., 2020c) Also, the ultrasonic treatment could have decomposed the molecular chains of EFBSNP by shearing and exposed the hydroxyl group. This enhanced the interaction between the EFBSNP and the alcohol molecules, leading to the destruction of the molecules in solution and recrystallization of the EFBSNP (Lin et al., 2020). Nevertheless, a residual amorphous phase remains after the temperature treatment (Drisko et al., 2015).

3.6. Chemical compound and structure

The functional group and chemical compound of the EFBA and EFBSNP were determined by FTIR (Fig. 6b). The EFBSNP demonstrated some structural differences compared to the EFBA. Considerable number of adsorption bands disappeared while some decreased. The band at 650–1368 cm^{-1} is a standard feature of SiO_2. The band at 776 cm^{-1} was ascribed to (-Si-O-Si) symmetric whereas the band at 1032.31 cm^{-1} to Si-OH stretching vibrational bond, which are the main peaks of SiO_2. The peak at 1742.32 cm^{-1} was attributed to the H-O-H of adsorbed water, which is because of –OH adsorption band (Jafari et al., 2014). Small band occurring at 3749 cm^{-1} was assigned to sequence in silanol group (Si-O-H) and hydrogen bonding of water to SiO_2. With increasing thermal treatment, the peak at 3749 cm^{-1} fades, the disappearance of the peak at higher temperature indicates the evolution of CO_2 at higher temperature (Fernandes et al., 2017). The gradual decrease in peak height at 1032.31 cm^{-1} with increasing temperature is due to the removal of physiosorbed water (Tettey and Lee, 2013). Initially, the amount of inaccessible silanol group increased but with increase in temperature, the isolated silanol group undergoes a condensation reaction to form siloxane bonds and water vapour as a by-product (Tettey and Lee, 2013). Consequently, the silanol peak reduced at temperatures above 700 °C. After thermal treatment up to 1200 °C, the silanol group may be present to some extent (Tettey and Lee, 2013). Nevertheless, –OH intensity at 1742.32 cm^{-1} shows an increase (EFBSNP) compared to EFBA. This could be attributed to the ultrasonic treatment as more free –OH groups are released with the decrease in size (Gu et al., 2020). The non-appearance of any other adsorption band indicates that it is pure SiO_2. Consequently, the position of the characteristic peaks is consistent which means that the synthesis method did not change the chemical composition.

3.7. Thermal properties results

The improvement of thermal properties of nanoparticles can prove uniform dispersion and their ability to interact with other materials (Borouni et al., 2018). Fig. 6c shows the thermal stability of EFBA and EFBSNP. The thermograms show distinct endothermic peaks. The first endothermic peak between 86.96 and 104.77 °C (Fig. 6c) was attributed to the evaporation of absorbed alcohol/water (Wang et al. 2010; Hossain et al., 2019). The second endothermic peak between 239.09 and 293.46 °C corresponds to the rupture of hydrogen bond, which was represented as Si-OH (Wang et al. 2010; Hossain et al., 2019). Consequently, the endothermic peaks of EFBSNP decrease compared to EFBA (Table 3), which could be due to the introduction of a more reactive surface as a result of the synthesis method (Singh et al., 2007). High temperature during thermal treatment supports the formation of crystalline phase due to the energy supplied to the system. Besides, during the wet milling, the ball mill strongly influences the kinetic transformation of amorphous phase to crystalline phase in a reaction and diffusion induced mechanisms (Borouni et al., 2018). Also, ultrasonic treatment might have decomposed the molecular chains of the EFBSNP by shearing, exposing the hydroxyl group, which enhanced the interaction between the EFBSNP and alcohol molecules leading to destruction of the molecules in solution and recrystallization of the EFBSNP. This suggests that EFBSNP acted as an additional nucleation site and agent by lowering the surface free energy barriers towards nucleation thus inducing crystallization. Similar result was reported by previous study of Han

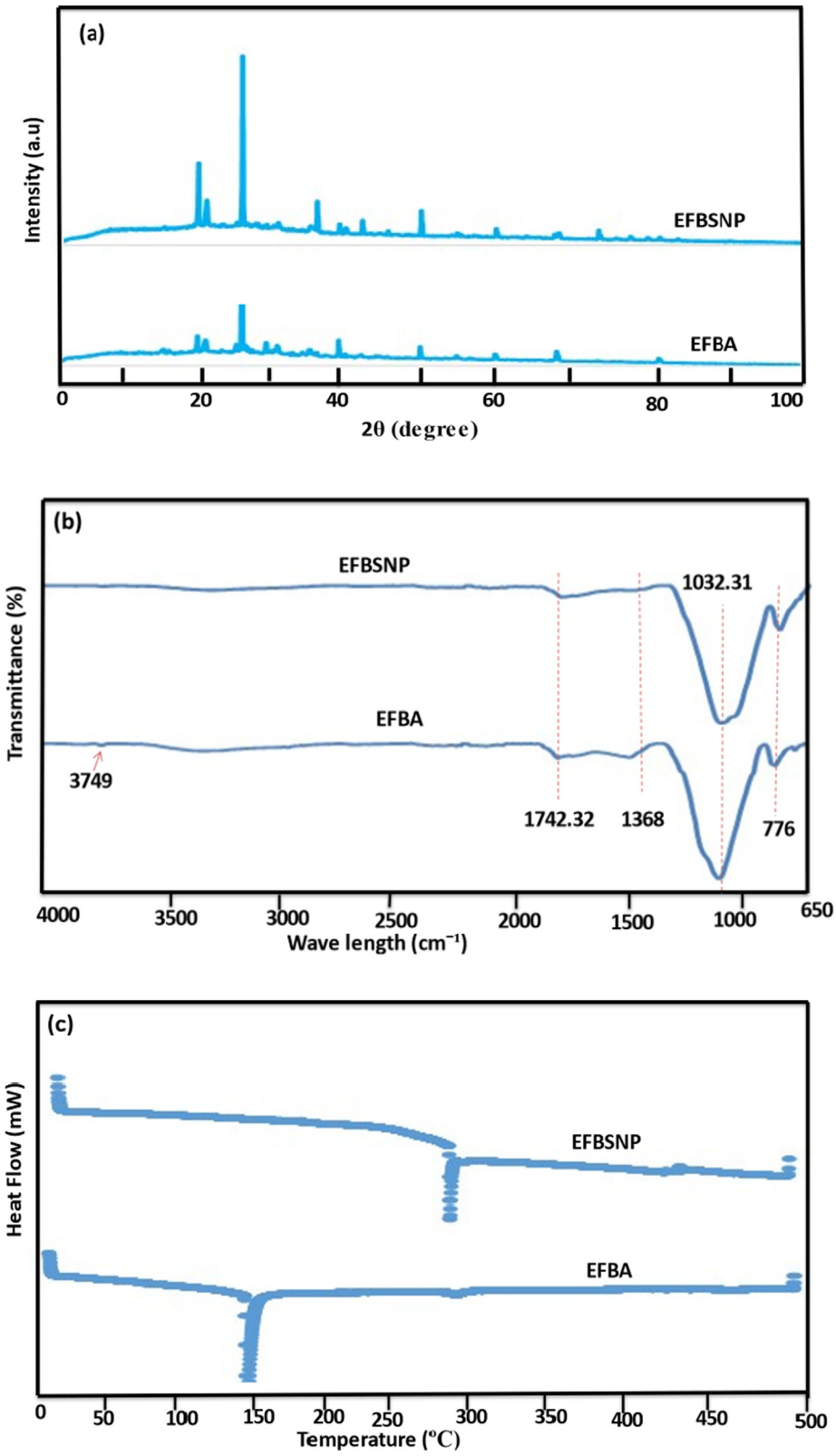

Fig. 6 (a) XRD results of EFBA and EFBSNP showing crystalline and amorphous phases (b) comparison of the FTIR spectra of EFBA and EFBSNP and (c) DSC thermograms of EFBA and EFBSNP showing different endothermic peaks.

et al. (2018) they stated that grafting of hydroxyl group on SiO_2 nanoparticles can improve its compatibility as a nucleating agent and improves its stability. This is consistent with the shift of the first endothermic peak of EFBSNP to higher temperatures compared to EFBA, implying that the ultrasonic treatment accelerated crystallization. Therefore, the higher rel-

Table 4 Summary of the thermal properties of EFBA and EFBSNP.

Samples	Glass Transition Temperature			Endotherm Peak I			Endotherm Peak II		
	Onset (°C)	Peak (°C)	Cryst (%)	Onset (°C)	Peak (°C)	Endset (°C)	Onset (°C)	Peak (°C)	Endset (°C)
EFBA	86.96	87.72	10	153.07	153.91	158.09	278.59	286.65	293.46
EFBSNP	104.11	104.77	46.78	236.79	221.43	212.48	280.61	281.32	283.23

ative crystallinity of EFBSNP compared to EFBA (Table 4) confirmed that EFBSNP acted as a nucleation site (Amigo et al., 2019). Subsequently, the glass transition temperature (Tg) of EFBSNP increased compared to EFBA. The increase in Tg indicates that a strong physical bond was formed between EFBSNP, hindering their movement at high temperatures (Hong et al., 2007). This implies that the mobility of EFBSNP subsequently decreased and became ordered (Soleimani and Mohammadi, 2018).

3.8. Surface chemical composition of EFBA and EFBSNP

XPS analysis was carried out to confirm the existence of silicon (Si) and oxygen (O) elements in EFBA and EFBSNP. Fig. 7 shows the survey and high-resolution spectra of Si (2p) and O (1s) indicating the presence of Si and O component of SiO_2 in EFBA and EFBSNP. It was observed that the surface composition of EFBSNP was similar to the bulk (EFBA) composition (Fig. 7a-b). Nevertheless, the major difference was observed in the peak occurring around 99 eV for EFBA (Fig. 7c) corresponding to the Si 2p orbit assigned to bulk Si and at 100 eV for EFBSNP (Fig. 7d) which was ascribed to SiO_2. The chemical shift to higher energies was due to the thick SiO_2 layer (Hou et al., 2017). This is because after wet milling, high concentration of SiO_2 was observed on the surface. Also, due to size reduction, the surface of Si was exposed and likely to form a SiO_2 layer as result of the reaction with ethanol during wet milling (Hou et al., 2017). This concurs with previous study of Krishnarao and Godkhindi (1992) they reported that the change in spectra could be because of the bonding of SiO_2 to organic material present in the EFBA. Fig. 7e and f shows the O 1s spectra for EFBA and EFBSNP. The peaks at 538 and 537 eV correspond to Si^{4+} core level in EFBA and EFBSNP, respectively. The shift in the O 1s peak to lower energies might be due to the reaction of Si with ethanol during wet milling resulting in the formation of Si-O-CH_2CH_3 on the surface of the EFBSNP (Hou et al., 2017).

3.9. Ultrasonic absorption performance of EFBSNP

The ability of EFBSNP to absorb ultrasonic waves was investigated. Figs. 8 and 9 show the performance at different concentration of EFBSNF in different fluids. The temperature of both medium (water and oil) increased with ultrasonication time (Figs. 8 and 9). This is because high energy output of ultrasonic energy increases the frictional limit, which led to an increase in the temperature of the samples. However, the addition of EFBSNP increased the temperature compared to water and oil alone. This is because energy is transferred to the medium (oil and water), during the ultrasonic process, resulting in cavitation within the medium. Cavitation energies help to disintegrate agglomerated particles through the reaction force of the bubble implosion. The shear effect created by the implosion increases the heat transfer and thus the temperature increases (Adio et al., 2016). In addition, the ultrasonic treatment increased the Brownian motion of the EFBSNP, which increased the probability of contact between the particles. The collision of the EFBSNP converted the potential energy of the particles into kinetic energy generating heat that increased the temperature of the system. Likewise, the high temperature increase is caused by attenuation of ultrasound energy however, the addition of EFBSNP changed the coefficient of the medium thereby increasing the rate of heating. This agrees with prior work of Sviridov et al. (2019) they reported that mesoporous silicon-based nanoparticles enhanced cavitation effect of ultrasound which led to additional heating of the surrounding and initiation of sonochemical reaction. Nevertheless, the higher temperature in deionized water compared to heavy oil is due to cavitation. Cavitation forms more easily in lighter fluids than in viscous fluids (Hamidi et al., 2014; Agi et al., 2019a). This is because the formation of cavitation in a liquid requires that the negative pressure in the rarefaction region be above the natural cohesive force acting in the liquid (Hamidi et al., 2014). Therefore, cavitation is less intense in viscous fluids where the forces are pronounced (Agi et al., 2019a). Furthermore, the higher temperature in EFBSNF could be due to the high surface charge of EFBSNP (Fig. 5d), which were immediately available for thermal interactions, leading to microconvection and increased heat transfer (Das et al., 2006). Therefore, it can be concluded that the temperature increase is dependent on ultrasonic cavitation and the increase in Brownian motion due to mechanical vibration. Absorption performance of EFBSNP increased with concentration, this is because of the high number of EFBSNP active site and sufficient surface available for absorption. However, above 0. 1 wt% the absorption rate diminished, this might be attributed to gradual saturated of the active site at higher concentration and lack of access to the active site. Similar result was reported by previous study by Montes et al. (2018) they observed a slight increase of only 2% at higher concentration. This signifies that the optimum concentration has been exceeded. Also, the effect of particle size on absorption of ultrasound in different fluids was investigated (Figs. 8 and 9). The EFBSNF showed higher absorption capacity compared to the EFBA in micron size. This could be attributed to the increase in surface area as the particle size decreased. Consequently, more particles were in solution for absorption of ultrasound. It might also be because of the increase in solubility with decreasing particles size (Sandri et al., 2013).

3.10. Effectiveness of EFBSNP in heavy oil viscosity reduction

The effects of different concentration of EFBSNF and ultrasound on the viscocity of heavy oil is shown in Fig. 10. The viscosity of the samples decreased with increasing ultrasonic

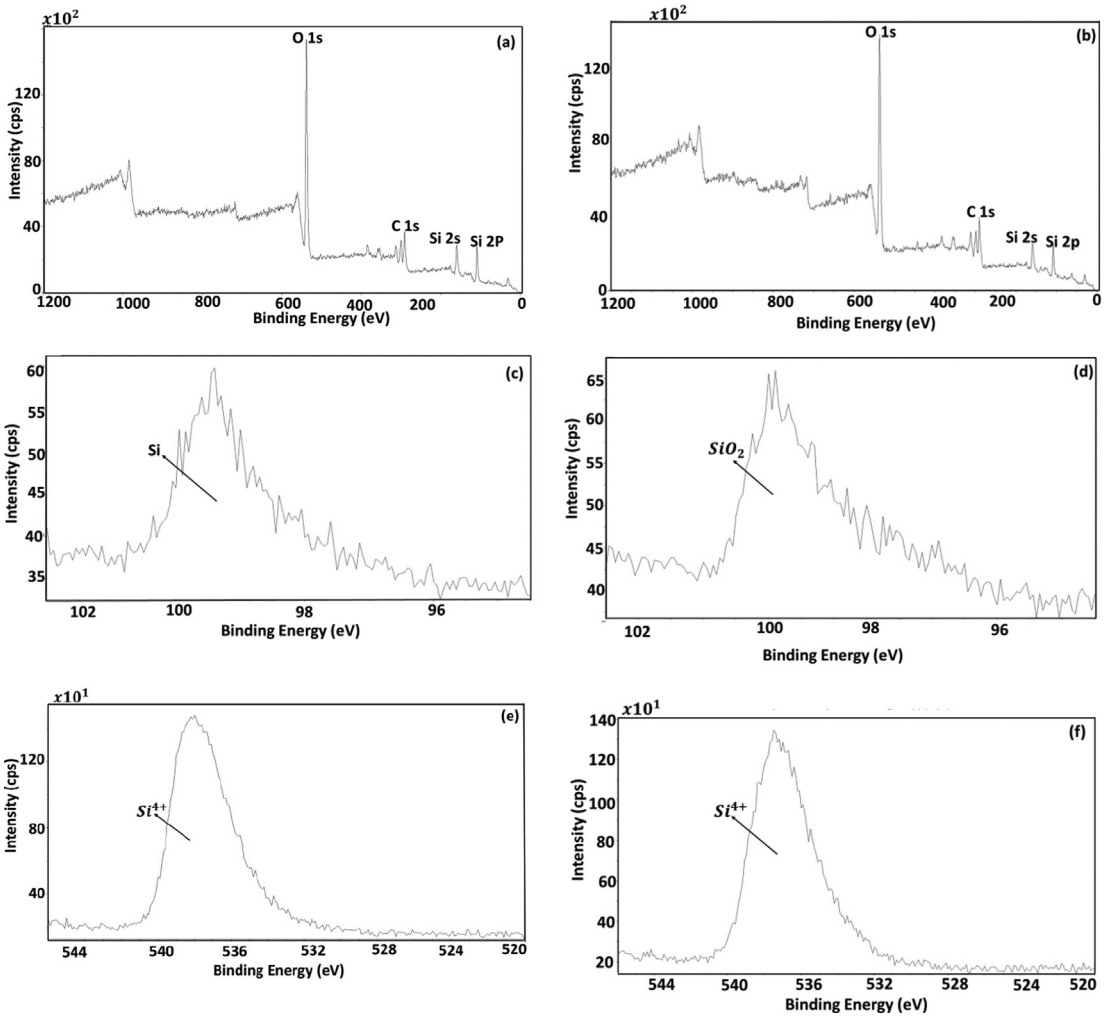

Fig. 7 XPS spectra for EFBA and EFBSNP: (a) survey of EFBA (b) survey of EFBSNP (c) high-resolution spectrum of peak Si 2p for EFBA (d) high-resolution spectrum of Si 2p peak for EFBSNP (e) high-resolution spectrum of O 1s peak for EFBA and (f) high-resolution spectrum of O 1s peak for EFBSNP.

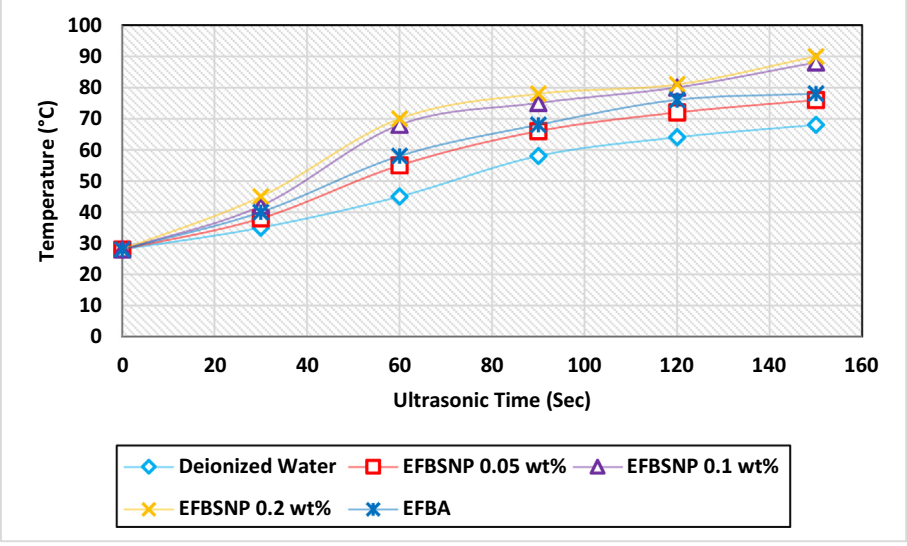

Fig. 8 Performance ability of EFBA (0.2 wt%) and EFBSNF to adsorb ultrasonic wave with time in deionized water.

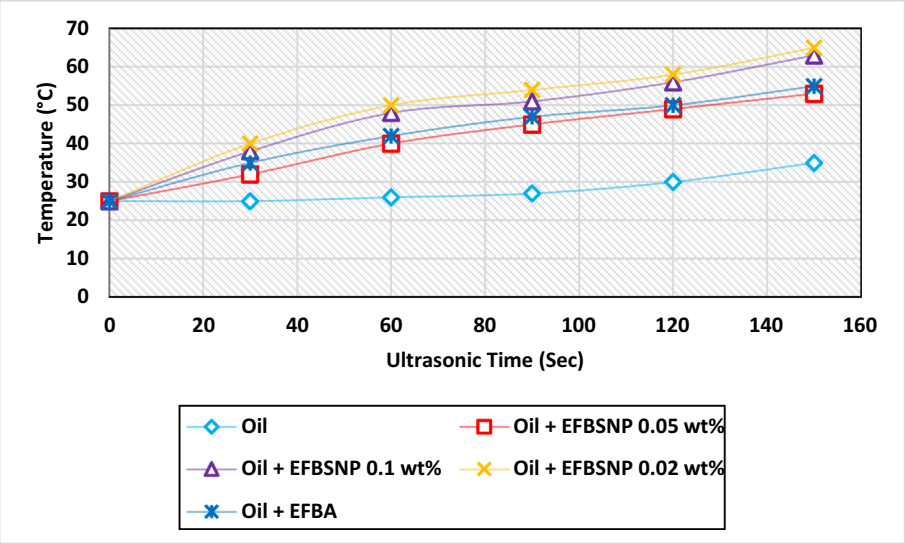

Fig. 9 Performance ability of EFBA (0.2 wt%) and EFBSNF to adsorb ultrasonic wave with time in heavy oil.

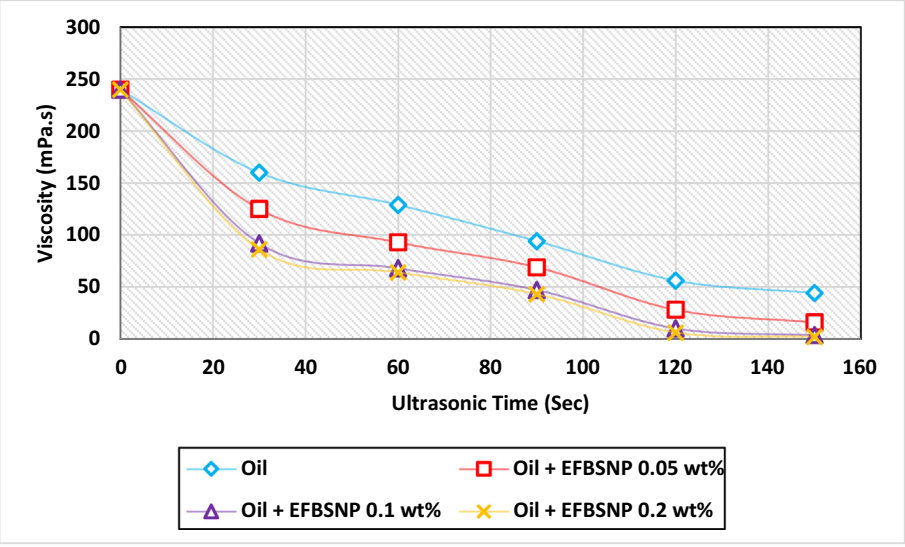

Fig. 10 Influence of EFBSNP in reducing the viscosity of heavy oil in the presence of ultrasound.

exposure time. This could be due to the fact that as the ultrasonic exposure time increases, a higher number of bubbles are involved in the cavitation process (Montes et al., 2018). Cavitation triggers a chemical reaction that breaks down high molecular weight compunds associated with the viscosity of heavy oil. Therefore, the cavitation effect generates high temperature, high pressure and micro jets that change the internal structure of the oil sample (Montes et al., 2018; Olaya-Escobar et al., 2020). Consequently, several macromolecules in the oil samples were broken-down into smaller fragments and carbon-carbon (C-C) bond of the heavy oil breaks to two free radicals compunds (R* and R'*) with lower molecular weight (Eq. (1)), reducing the viscosity. Also, both hydrogen and hydroxyl radicals are produced during the homolytic dissassociation of water molecules (Eq. (2)). Consequently, hydroxyl radical reacts with alkane (abstraction reaction) to form a new alkyl radical (Eq. (3)) (Lin and Yen, 1993).

$$RR' \rightarrow R^{*}R'^{*} \tag{1}$$

$$H_2O \rightarrow H^{*} + OH^{*} \tag{2}$$

$$RH + OH^{*} \rightarrow H_2O + R^{*} \tag{3}$$

$$H_2 \rightarrow 2H^{*} \tag{4}$$

Therefore, hydrogen radical may come from water or dissolved hydrogen by ultrasound (Eq. (4)). However, when ultrasound alone was applied, the effect of droplet coalescence was minimal and fewer hydrogen free radicals were produced during the cracking reaction (Montes et al., 2018). Hence, when few hydrogen free radical are produced, the large molecule free radical will experience acumulation to bigger structure impeding viscosity reduction and heavy oil modification (Wan et al., 2019). However, with the addition of EFBSNF, functional

hydrogen radical were generated through cavitational impact to end the movement of the macromolecules free radicals. In this way, alkyl radical was terminated by reaction with hydrogen radical (Equation (5)). In similitude, the hydrogen radical reacted with hydroxly or hydrogen radical to form water or hydrogen molecule (Eqs. (6) and (7)). The viscosity of the heavy oil decreased further with increase in concentration of EFBSNP, which might be attributed to the availability of the dissociated hydrogen to freely interact with the macromolecular free radical thereby, preventing growth of the heavy oil, inhibit condensation reaction, promote hydrogenation reaction, improve the quality of the heavy oil and further reduce viscosity.

$$R^* + H^* \rightarrow RH \tag{5}$$

$$H^* + OH^* \rightarrow H_2O \tag{6}$$

$$H^* + H^* \rightarrow H_2 \tag{7}$$

3.10.1. Possible mechanisms for EFBSNF assisted ultrsound in viscosity reduction

Under EFBSNF ultrasound assisted cavitation reaction, the mechansims of thermal scission and generation of free radical mechanisms may occur simultaneously. Thermal scission mechanism causes heavy oil molecules to break into lighter fraction of gas oil. Whereas generation of free radical mechanism provides a source for the hydrogenation of heavy oil (Lin and Yen, 1993). Therefore, the mechansims of viscsoity reduction of heavy can be divided into three process:

(i) Generation: In the generation stage, the C-C bond of heavy oil macromolecules are broken down to form free radicals through the high temperature and pressure of ultrasound cavitation (Equations (1) and (2)).

(i) (ii) Propagation: During the propagation reaction, hydrogen transfer reaction occurs whereby the free radicals takes hydrogen from other hydrocarbon molecules to form new free radicals (Eq. (3)). Also, these free radical might undergo decompostion, addition or isomerization to form stable molecules which might impede the viscsoity reduction by ultrasound alone.

(ii) Termination: The further decrease in viscsoity by EFBSNF addition is through the termination reaction of the stable molecules (Eqs. (5) and (6)).

3.11. Effect of temperature rise on interfacial tension (IFT)

The temperature rise can affect the fluid properties such as IFT and viscosity. The IFT between EFBSNF (0. 1 wt%) and heavy oil was calculated using Firoozabadi and Ramey's Equation (8) (Firoozabadi and Ramey, 1988; Agi et al., 2018).

$$\sigma^{1/4} = \frac{a_1 \Delta\rho^{b_1}}{T_r^{0.3125}} \tag{8}$$

$$\Delta\rho = \rho_w - \rho_{ho} \tag{9}$$

$$\Delta\rho = \rho_{nf} - \rho_{ho} \tag{10}$$

$$\sigma = \left[\frac{1 - (\Delta\rho) + 1.76}{T_r^{0.3125}}\right]^4 \tag{11}$$

whereas σ is IFT (mN/m), T_r is critical temperature (°C), a_1 and b_1 are constants (mN/m), ρ_w ρ_{nf} and ρ_{ho} are density of water, nanofluid (0.1 wt%) and heavy oil (g/cm^3), respectively. Generally, high IFT and viscous forces prevail at low temperature, and IFT decreases with increasing temperature (Fig. 11). Fig. 11 shows that IFT decreased to 0.2 mN/m compared to 0.9 mN/m with only ultrasound, this might be attributed to aqauthermolysis mechansim. Thermal energy from ultrasound can crack some of the compunds in the heavy oil however, cracking of larger molecules is minimal. In the presence of EFBSNF the interfacial area increases thereby improving the cracking of heavy oil as most cracking reaction takes place at oil-water (O/W) interface during aquathermolysis (Wang et al., 2014). This concur with prior work of Li et al. (2021), they reported that ultrasonic wave is capable of changing the oil components through aquathermolyis, heating effect and the intermolecular forces become weak due to the incresaing molecular distance thus lowering the IFT. Furthermore, the kinetic energy of EFBSNF increased with temperature, therefore, more particles migrate to the interface and the number of surface active agents at the interface increased. As the temperature increased, the vapour pressure of the medium and nuclei increased, resulting in cavitation (Agi et al.,2020a). At high ultrasound, coalescence occurs due to collisions of dispersed EFBSNF, acoustic flow and Bjerkenes forces (attractive forces between the oscillating droplet and heat due to ultrasound). As a result, stresses occur at the interface due to expansion and compression, which overcome the interacting forces holding the large droplet, causing it to break, into smaller droplets and reducing the IFT.

3.11.1. Possible mechanisms for EFBSNF assisted ultrasound in IFT reduction

Fig. 12 depicts the schematic illustration of the possible mechanisms that aided IFT reduction during the EFBSNF assisted ultrasound process. Fig. 12 shows that cavitation helps in the separation of phases exposed to ultrasound. Since the EFBSNP tends to drift towards the O/W interface, the high temperature reduces the rigidity at the interface, making it easier for the droplet to coalesce upon collision. Ultrasound facilitated the adsorption of EFBSNP droplets at the interface forming an interfacial film. Ultrasonication might have stimulated the interfacial film making it more hydrophobic enabling the EFBSNF to adsorb faster at the O/W interface to form a layer (Fig. 12b) which increased the potential between the EFBSNP and imparted a repulsive force between them. Compression and expansion bring stress to O/W interface during ultrasound application, overcoming the linked forces that hold large droplets together and breaking them into smaller ones (Agi et al., 2020c). Hence, O/W boundary was replaced by EFBSNF consequently, a hydrophilic/water and hydrophobic/oil interfaces was formed. The repulsive force was induced by the hydroxyl group of EFBSNP which bonded together with water while the hydrophobic component reacts with oil causing inter-molecular O/W integrated force to reduce thus, decreasing IFT (Sukmarani and Ledyastuti, 2019; Agi et al., 2020a; 2021). In similitude, Sukmarani and Ledyastuti (2019) stated that hydroxyl group can easily bind to water thereby

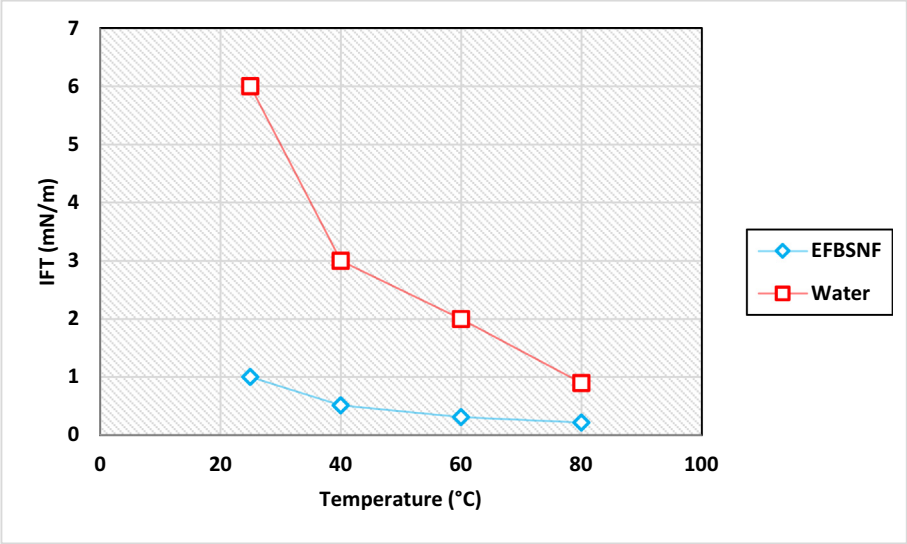

Fig. 11 Ability of EFBSNF in reducing IFT of heavy oil as a function of temperature.

decreasing IFT. Consequently, rapid adsorption of EFBSNP at hydrophobic interfacial film was enabled, which induced steric and electrostatic interactions that synergistically reduced the IFT (Agi et al., 2020b). As a result, the entropy of the whole suspension increases due to the increase in the freedom of EFBSNP, leading to a decrease in Gibbs free energy (Eq. (12)). The decline in Gibbs free energy reduces the free energy at the surface thus, decreasing the IFT (Eq. (13)) (Agi et al., 2020a).

$$\Delta G = \Delta H - T\Delta S \tag{12}$$

$$\Delta G = \gamma \partial A(constant T \& P) \tag{13}$$

whereas ΔG is difference in Gibbs free energy (Kj mol^{-1}), ΔS is difference in entropy ($J.K^{-1}$), ΔH is difference in enthalpy (KJ), P is pressure (Pa), T is temperature (K) and γ is free energy at O/W interface (N/m). A decrease in IFT reduces the capillary pressure generated by the trapped oil droplets in the pores, effectively mobilizing the oil.

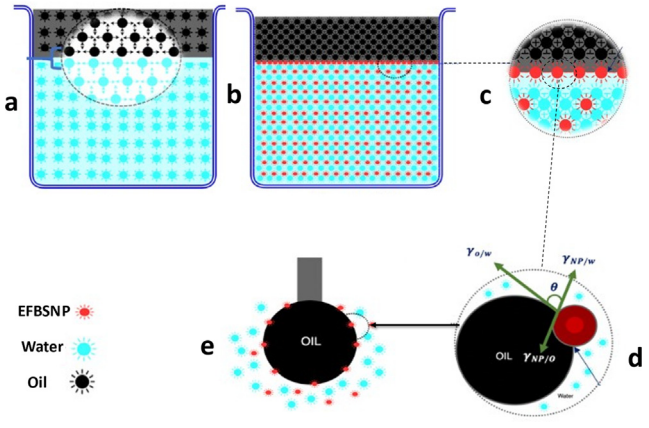

Fig. 12 Schematic illustration of IFT reduction between O/W by EFBSNF (a) IFT of O/W due to unbalanced forces (b) oil and EFBSNF with ultrasound (c) adsorption of EFBSNP at O/W interface (d) decrease in is free energy at O/W interface and (e) decrease in IFT.

3.12. Nanofluid oil displacement without ultrasound

Six different sand packs were used for the initial series of tests (Table 2) to investigate the efficiency of EFBSNF in heavy oil recovery at different concentration (Fig. 13). About 24.5% original oil in place (OOIP) was recovered by waterflooding. This indicates the inefficiency of waterflooding in recovering heavy oil, which can be attributed to viscous fingering and early water breakthrough. Therefore, EFBSNF flooding was investigated to recover the bypassed oil. As a result, the oil recovery increased by 20.5%, 26.33% and 28.5% with 0.05 wt%, 0.1 wt% and 0.2 wt% EFBSNF, respectively (Fig. 13). This increase can be attributed to the improvement in the flow properties of the porous medium as the EFBSNP plugged the channels created by the waterflooding (Cheraghian and Tardasti, 2012; Cheraghian et al., 2020). This resulted in uniform sweep efficiency and hence increased oil recovery (Cheraghian, 2016; Nezhad and Cheraghian, 2016). In addition, flooding with EFBSNF caused a change in the viscous force distribution that had occurred during the initial waterflooding (viscosity difference). These changes resulted in a more stable displacement front due to the reduction in viscosity. Similar result was reported by previous work of Cheraghian et al. (2017) they stated that SiO_2 nanoparticles can modify the flow of displacing fluid due to the change in viscosity. The results are consistent with the efficiency of viscosity reduction by EFBSNF (Fig. 10). Oil recovery increased with concentration of EFBSNF due the increase in viscosity of the nanofluids which mobilize the bypassed oil. However, at higher concentration, the increase in oil recovery was minimal which might be due to pore blocking.

3.13. Ultrasound assisted nanofluid flooding

The optimum concentration of 0.1 wt% EFBSNF was used for the ultrasound experiment. Ultrasound-assisted EFBSNF

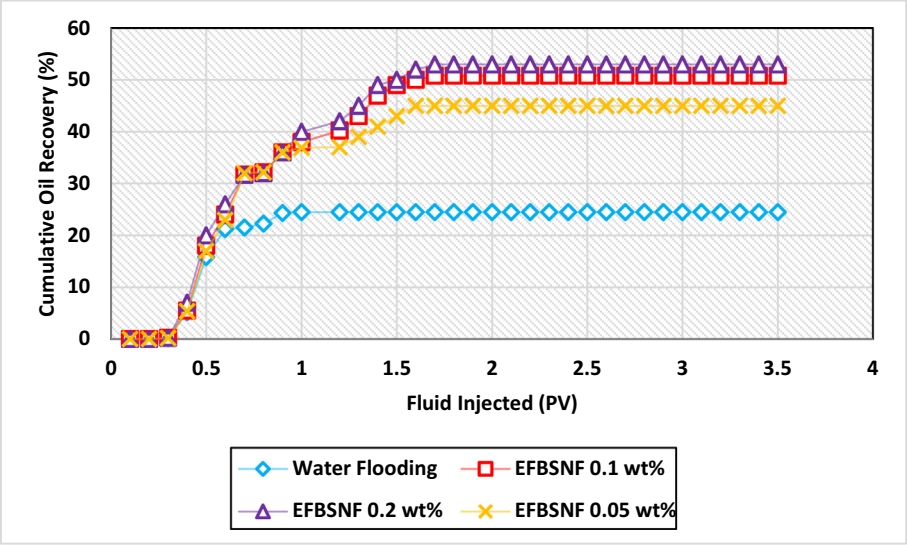

Fig. 13 Oil recovery efficiency of EFBSNF at different concentrations.

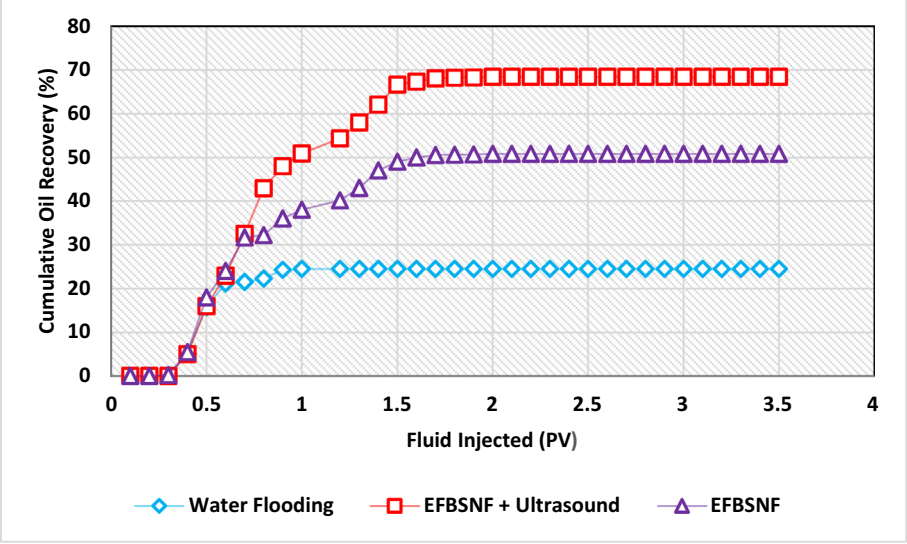

Fig. 14 Oil recovery efficiency of 0.1 wt% EFBSNF with and without ultrasound compared to water flooding.

flooding was used as a tertiary oil recovery method and the results obtained were compared with the first set of experiments without ultrasound. Fig. 14 shows that ultrasound assisted EFBSNF flooding recovered 44.3% OOIP, increasing oil recovery by 18% compared to oil recovery without ultrasound. This is due to the fact that ultrasound caused rapid movement of trapped oil, which was initially bypassed by waterflooding and EFBSNF flooding (Agi et al., 2019c). This movement caused the high molecules of the heavy oil to break up, thereby increasing their mobility (Agi et al.,2018). Similarly, it could be due to the attractive forces between the oscillating oil droplets (Bjerknes forces), leading to coalescence of smaller oil droplets into a single stream with higher mobility thereby, flowing out of the porous medium (Agi et al. 2018). In addition, ultrasound interacts with the intermolecular forces that set it in motion (Brownian forces), and the ultrasonic vibration of EFBSNF causes stresses that led to an increase in pressure and temperature. This is consistent with the pressure drop profile (Fig. 15), as ultrasound assisted EFBSNF flooding showed a higher pressure drop compared to EFBSNF flooding without ultrasound. This high pressure drop indicates a more stable displacement and lower viscosity pushing the oil ahead of the EFBSNF (Hamidi et al., 2017). Nevertheless, the pressure dropped back to lower values after reaching a peak (Fig. 15). This is due to the cavitation effect, where a high-pressure surge is generated in the system during the implosion of the bubbles. However, after the bubble implosion the pressure drops as shown in Fig. 15 (Mohammadian et al., 2013). Furthermore, the temperature rise might have increased the surface activity and hydrophobicity at the interface, reducing

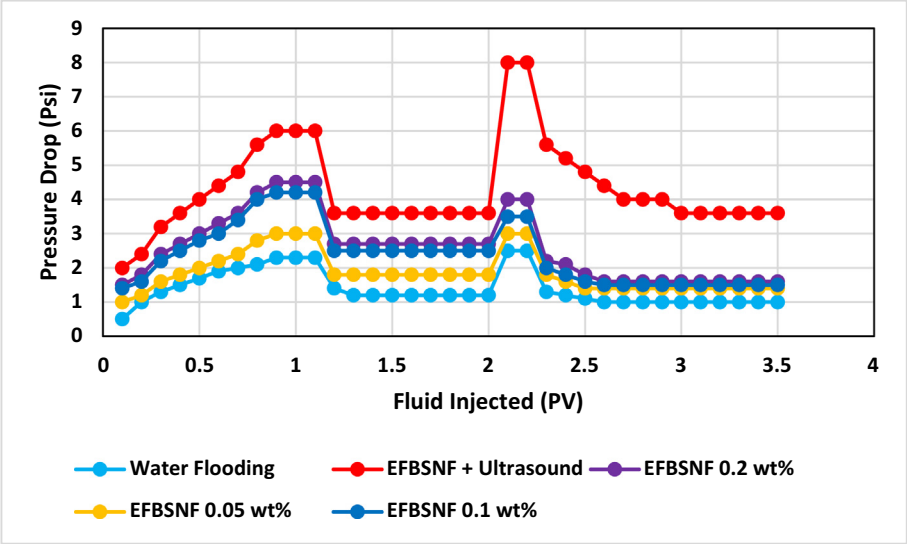

Fig. 15 Pressure drop profile of EFBSNF flooding with and without ultrasound compared to water flooding.

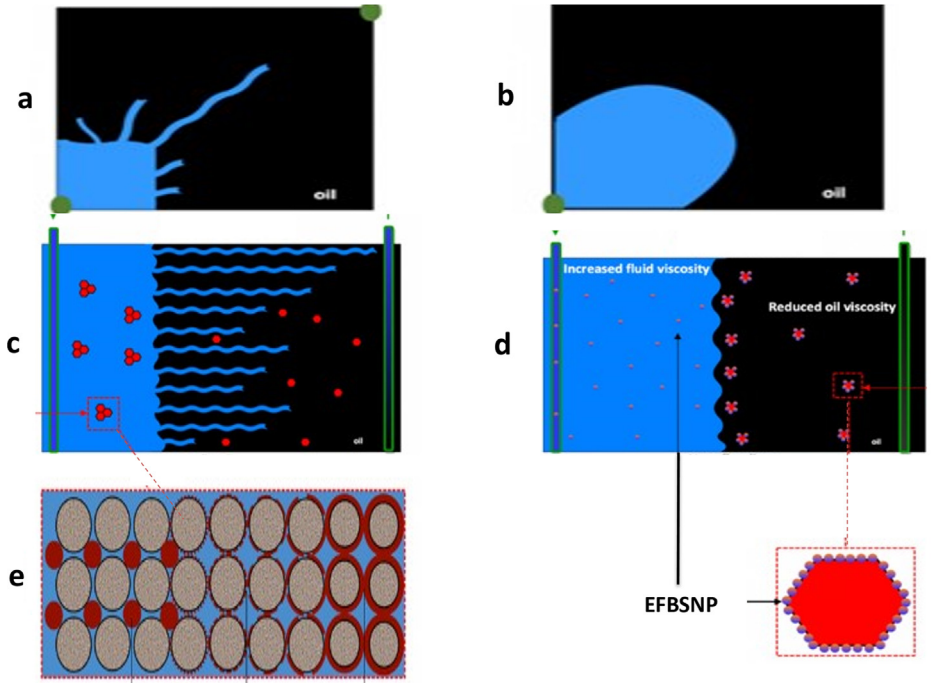

Fig. 16 Schematic illustration of heavy oil recovery process using EFBSNF and Ultrasound (a) viscous fingering during water flooding (b) piston like font during EFBSNF flooding assisted with ultrasound (c) precipitation and deposition of heavy oil molecules during water flooding resulting in ununiform sweep efficiency (d) EFBSNP and ultrasound breakdown large molecules of heavy oil and reduced viscosity of heavy oil and (e) heavy oil molecules deposition.

the IFT, thereby, resulting in increased oil recovery. As a result, the aqueous phase flows (peristaltic motion) rather than adhering to the porous media (Agi et al., 2019b).

3.13.1. Possible mechanisms for EFBSNF assisted ultrasound oil recovery

The possible heavy oil recovery mechanisms were proposed based on heavy oil displacement experimental results. Fig. 16 depicts the schematic illustration of the possible oil recovery mechanisms during EFBSNF assisted flooding. For effective heavy oil recovery, deformation is required for trapped oil to move through the pore throat. The deformation was aided by the reduction of the O/W IFT. The degree of residual oil mobilization in porous media is determined by the mobility ratio (Eq. (14)). Fig. 16a shows that flooding with water could not mobilize the trapped oil and the mobility ratio (M) is greater than 1. This means that the mobility of water is higher than that of the heavy oil ($M > 1$), an adverse event known as viscous fingering (Fig. 16c). This can be attributed to the high

Table 5 Energy and cost estimation of the EFBSNF assisted ultrasound oil recovery.

Material and process	Energy utilized (kwh)	Cost (US$/kg)
EFB	–	–
Ethanol	–	2.2/gallon
Heating	1.5	0.0795
Size Reduction	5.25	0.0278
Drying	12.5	0.662
Ultrasonication	605	32
Miscellaneous	–	10
Total	624.25	44.96

viscosity of the heavy oil hence a mobility ratio of less than 1 cannot be achieved resulting in early breakthrough and poor recovery during water flooding (Fig. 16c). This poor recovery might be due to precipitation and deposition of the heavy oil molecules (Fig. 16c). The precipitation and deposition of heavy oil molecules might be due to the changes in crude oil pressure during the waterflooding (Yakasai et al., 2021). However, Fig. 16b shows that the EFBSNF-assisted ultrasound had a piston like dispalcement shape indicating that the $M \leq 1$. This confirms the ability of EFBSNF flooding assisted ultrasound to simultaneously increase the viscosity of the injection fluid and also minimise the heavy oil viscosity. However, the reduction is higher with ultrasound due to the stronger effect of aquathermolysis catalysed in the presence of EFBSNF (Fig. 16d), resulting in uniform, efficient and increased oil recovery (Farooqui et al., 2015). During the EFBSNF flooding, the EFBSNF acted as inhibitor to prevent the heavy oil from precipitation by adsorbing the molecules. The breakdown of these heavy oil molecules resulted in the reduction in viscosity of the heavy oil thereby preventing aggregation, precipitation and deposition of the heavy oil molecules on the rock surface. In combination with ultrasound the reaction of the EFBSNF increased by creating more active surface for contact with the heavy oil molecules, which is consistent with viscosity results (Fig. 10).

$$Mobility\ \ ratio(M) = \frac{K_{rd}}{K_{ro}} \times \frac{\mu_o}{\mu_d} \tag{14}$$

whereas K_{rd} is relative permeability of displacing fluid, K_{ro} is relative permeability of displaced fluid, μ_o and μ_d are viscosity of displaced fluid and displacing fluid, respectively.

3.14. Economic feasibility

The energy and cost of the process was estimated using Eqs. (15) and (16).

$$E = Pt \tag{15}$$

$$Cost = E(cost1kwh) \tag{16}$$

whereas E is electrical energy (kwh), P is power of electrical appliances (kwh), t is time of electricity consumption (h). Table 5 shows the energy utilization and cost of EFBSNF assisted ultrasound oil recovery process. The energy utilization and cost estimation of producing EFBSNP was less than the chemical treatment method (US$63.03–92.98) (Nayak et al., 2019). This cost may reduce further if EFBSNP is produced in commercial scale. The upscaling of ultrasound equipment is easy and cost effective this has enabled the sonochemical treatment of oil wells in Western Siberia and Samara Region (Abramov et al., 2015; 2017). The treatment method decreased sonication time from an hour and above to 30 min, increased the duration of the effect and increased production (Abramov et al., 2015; 2017; Mullakaev et al., 2017). However, acids, oxidants, enzymes and chelates were the chemical used for treatment. The use of some of these chemicals is in contrasts with ultrasound methods as environmentally friendly approach. EFBSNP is cost effect and environmentally friendly hence it can be used as substitute to the current EOR chemicals. The energy utilization and cost estimation indicted that this sonochemical method is cost effective and financially feasible.

4. Limitations and recommendation

The experiment was performed with an unconsolidated sandstone porous media with high porosity and permeability. Hence, future research work with reservoir sandstone core with medium to low permeability and porosity is recommended.

5. Conclusions

In this work, thermally treated EFBSNP was produced by ultrasound-assisted wet-milling and their effectiveness in enhancing cavitation effect of ultrasound to improve heavy oil recovery was evaluated. From the findings of this research, the resulting important inferences were identified. The treatment method showed a significant decrease in the concentration of the trace element with increasing temperature and a corresponding increase in SiO_2 content. Similarly, the non-appearance of any other adsorption band in the FTIR spectra indicates that it is pure SiO_2, and the position of the characteristic's peaks is consistent, confirming that the synthesis method did not change the chemical composition. The change in size and shape during the thermal treatment of EFBA had no effect on the resultant EFBSNP after wet milling but rather it increased the surface stability resulting to the formation of crystalline phases of quartz and tridymite. The combined effect of EFBSNF and ultrasound reduced the viscosity of the heavy oil through the mechanism of thermal scission and generation of free radical. The EFBSNF assisted-ultrasound lowered the IFT to an extremely low value (0.2 mN/m), which effectively mobilized the trapped oil droplets in the pores through the mechanism of aquathermolysis. Ultrasound-assisted EFBSNF flooding increased oil recovery by 44.33% compared to oil recovery without ultrasound which increased by 26.33% through the mechanism of Bjerknes forces and peristaltic motion.

Declaration of Competing Interest

The authors declare that they have no known competing financial interests or personal relationships that could have appeared to influence the work reported in this paper.

Acknowledgement

The authors are grateful to Ministry of Higher Education, Malaysia and UTM (Q.J130000.3551.07G12;R.J130000.7851.5F030;Q.J1300003551.06G68;R.J1300007351.4B545).

Appendix A. Supplementary data

Supplementary data to this article can be found online at https://doi.org/10.1016/j.arabjc.2022.103784.

References

Abramov, V.O., Abramova, A.V., Bayazitov, V.M., Altunina, L.K., Gerasin, A.S., Pashin, D.M., Mason, T.J., 2015. Sonochemical approaches to enhanced oil recovery. Ultrason. Sonochem. 25, 76–81.

Abramov, V.O., Abramova, A.V., Bayazitov, V.M., Mullakaev, M.S., Marnosov, A.V., Ildiyakov, A.V., (2017) Acoustic and sonochemical methods for altering the viscosity of oil during recovery and pipeline transportation. Ultrasonics Sonochemistry 35 (Part A): 389-396.

Adio, S., Sharifpur, M., Meyer, J., 2016. Influence of ultrasonication energy on the dispersion consistency of Al2O3–glycerol nanofluid based on viscosity data, and model development for the required ultrasonication energy density. J. Exp. Nanosci. 11 (8), 630–649.

Agi, A., Junin, R., Chong, A., 2018. Intermittent ultrasonic wave to improve oil recovery. J. Petrol. Sci. Eng. 166, 577–591.

Agi, A., Junin, R., Gbadamosi, A., Abbas, A., Azli, N.B., Oseh, J., 2019a. Influence of nanoprecipitation on crystalline starch nanoparticle formed by ultrasonic assisted weak-acid hydrolysis of cassava starch and the rheology of their solutions. Chem. Eng. Processing-Process Intensification 142, 107556.

Agi, A., Junin, R., Syamsul, M., Chong, A., Gbadamosi, A., 2019b. Intermittent and Short Duration Ultrasound in a Simulated Porous Media. Petroleum 5 (1), 42–51.

Agi, A., Junin, R., Shirazi, R., Gbadamosi, A., Yekeen, N., 2019c. Comparative Study of Ultrasound Assisted Water and Surfactant Flooding. J. King Saud University – Eng. Sci. 31 (3), 296-303.

Agi, A., Junin, R., Abdullah, M.A., Jaafar, M.Z., Arsad, A., Wan Sulaiman, W.R., Mohd Norddin, M.N.A., Abdurrahman, M., Abbas, A., Gbadamosi, A., Azli, N.B., 2020a. Application of Polymeric Nanofluid in Enhancing Oil Recovery at Reservoir Condition. J. Petrol. Sci. Eng. 194, 107476.

Agi, A., Junin, R., Jaafar, M.Z., Mohsin, R., Arsad, A., Gbadamosi, A., Fung, C.K., Gbonhinbor, J., 2020b. Synthesis and Application of Rice Husk Silica Nanoparticles for Chemical Enhanced Oil Recovery. J. Mater. Res. Technol. 9 (6), 13054–13066.

Agi, A., Junin, R., Arsad, A., Abbas, A., Gbadamosi, A., Azli, N.B., Oseh, J., 2020c. Ultrasonic-assisted Weak-acid Hydrolysis of Crystalline Starch Nanoparticles for Chemical Enhanced Oil Recovery. Int. J. Biol. Macromol. 148, 1251–1271.

Agi, A., Junin, R., Jaafar, M.Z., Sidek, M.A., Yakasai, F., Gbadamosi, A., Oseh, J., 2021. Formulation of bionanomaterials: a review of particle design towards oil recovery applications. J. Ind. Eng. Chem. 98, 82–102.

Ahmad, M., Gani, A., Hassan, I., Huang, Q., Shabbir, H., 2020. Production and characterization of starch nanoparticles by mild alkali hydrolysis and ultra-sonication process. Scientific Report 10, 3533.

Ali, J.A., Kolo, K., Manshad, A.K., Stephen, K., 2021. Emerging applications of TiO2/SiO2/poly(acrylamide) nanocomposites within the engineered water EOR in carbonate reservoirs. J. Mol. Liq. 322 (15), 114943.

Amigo, N., Palza, H., Canales, D., Sepulveda, F., Vasco, D.A., Sepulveda, F., Zapata, P.A., 2019. Effect of starch nanoparticles on the crystallization kinetics and photodegradation of high density polyethylene. Compos. B Eng. 174, 106979.

Asl, H.F., Zargar, G., Manshad, A.K., Takassi, M.A., Ali, J., Keshavarz, A., 2020. Effect of SiO2 nanoparticles on the performance of L-Arg and L-Cys surfactants for enhanced oil recovery in carbonate porous media. J. Mol. Liq. 300, 112290.

ASTM E 2161-08 Standard Terminology Relating to Performance Validation in Thermal Analysis.

Borouni, M., Niroumand, B., Maleki, A., 2018. A study on crystallization of amorphous nano silica particles by mechanical activation at the presence of pure aluminum. J. Solid-State Chem. 263, 208–215.

Chakraborty, S., Panigrahi, P.K., 2020. Stability of nano fluid: A review. Appl. Therm. Eng. 174, 115259.

Chen, G., Gao, J., Xu, L., Fu, X., Yin, Y., Wu, S., Qin, Y., 2012. Optimizing conditions for preparation of MnOx/RHA catalyst particle for the catalytic oxidation of NO. Adv. Powder Technol. 23 (2), 256–326.

Cheraghian, G., Tardasti, S., 2012). Improved Oil Recovery by the Efficiency of Nano-particle in Imbibition Mechanism. European Association of Geoscientists & Engineers. Conference Proceedings, 2nd EAGE International Conference KazGeo, 315-00078.

Cheraghian, G., 2016. Improved Heavy Oil Recovery by Nanofluid Surfactant Flooding - An Experimental Study. European Association of Geoscientists & Engineers, Conference Proceedings, 78th EAGE Conference and Exhibition, pp. 1–5.

Cheraghian, G., Kiani, S., Nassar, N., Alexander, S., Barron, A., 2017. Silica Nanoparticle Enhancement in the Efficiency of Surfactant Flooding of Heavy Oil in a Glass Micromodel. Ind. Eng. Chem. Res. 56 (30), 8528–8534.

Cheraghian, G., Rostamin, S., Afrand, M., 2020. Nanotechnology in Enhanced Oil Recovery. Processes 8, 1073.

Das, S., Choi, S., Patel, H., 2006. Heat Transfer in Nanofluids—A Review. Heat Transfer Eng. 27 (10), 3–19.

Drisko, G., Carettero-Genevrier, A., Perrot, A., Gich, M., Gazquez, J., Rodriguez-Carvajal, J., Favre, L., Grosso, D., Boissière, C., Sanchez, C., 2015. Crystallization of hollow mesoporous silica nanoparticles. Chem. Commun. 51, 4164–4167.

Farooqui, J., Babadagli, T., Li, H.A., 2015. Improvement of the recovery factor using nano-metal particles at the late stages of cyclic steam stimulation. Society of Petroleum Engineers - SPE Canada Heavy Oil Technical Conference, 601–617.

Fernandes, I.J., Sanchez, F., Jurado, F., Kieling, A., Rocha, T., Maraes, C., Sousa, V., 2017. Physical, Chemical and Electrical Characterization of Thermally Treated Rice Husk Ash and Its Potential Application as a Ceramic Raw Material. Adv. Powder Technol. 28, 1228–1236.

Firoozabadi, A., Ramey, H.J., 1988. Surface Tension of Water Hydrocarbon System at Reservoir Condition. J. Can. Pet. Technol. 27 (3), 41–48.

Gbadamosi, A., Junin, R., Manan, M., Agi, A., Oseh, J., Usman, J., 2019a. Effect of aluminium oxide nanoparticles on oilfield polyacrylamide: Rheology, interfacial tension, wettability and oil displacement studies. J. Mol. Liq. 296, 111863.

Gbadamosi, A., Junin, R., Manan, M., Agi, A., Oseh, J., Usman, J., 2019b. Synergistic application of aluminium oxide nanoparticles and oilfield polyacrylamide for enhanced oil recovery. J. Petrol. Sci. Eng. 182, 106345.

Gokce, Y., Cengiz, B., Yildiz, N., Calimli, A., Aktas, Z., 2014. Colloids and Surface A: Physiochemical and Engineering Aspects 462, 75–81.

Gu, H., Gao, X., Zhang, H., Chen, K., Peng, L., 2020. Fabrication and characterization of cellulose nanoparticles from maize stalk pith via ultrasonic-mediated cationic etherification. Ultrasonic Sonochemistry 66, 104932.

Han, Z., Wang, Y., Wang, J., Wang, S., Zhuang, H., Liu, J., Huang, L., Wang, Y., Wang, W., Belfiore, L.A., Tang, J., 2018. Preparation of Hybrid Nanoparticle Nucleating Agents and Their Effects on the Crystallization Behavior of Poly(ethylene terephthalate). Materials 11 (4), 587.

Hamidi, H., Haddad, A., Mohammadian, E., Rafati, R., Azdapour, A., Ghari, P., Ombewa, P., Neuert, T., Zink, A., 2017. Ultrasound-assisted CO2 flooding to improve oil recovery. Ultrason. Sonochem. 35, 243–250.

Hamidi, H., Mohammadian, E., Junin, R., Rafati, R., Manan, M., Azdarpour, A., Junid, M., 2014. A Technique for Evaluating the Oil/Heavy-Oil Viscosity Changes Under Ultrasound in a Simulated Porous Medium. Ultrasonics 54, 655–662.

Hossain, S., Mathur, K., Bhardwaj, A., Roy, P., 2019. A facile route for the preparation of silica foams using rice husk ash. Int. J. Appl. Ceram. Technol. 1–9.

Hong, R., Fu, H., Zhang, Y., Liu, L., Wang, J., Li, H., Zheng, Y., 2007. Surface-Modified Silica Nanoparticles for Reinforcement of PMMA. J. Appl. Polym. Sci. 105, 2176–2184.

Hou, S., Su, Y., Chang, C., Hu, C., Chen, T., Yang, S., Huang, J., 2017. The synergistic effects of combining the high energy mechanical milling and wet milling on Si negative electrode materials for lithium ion battery. J. Power Sources 349, 111e120.

Huang, X., Zhou, C., Suo, Q., Zhang, L., Wang, S., 2018. Experimental study on viscosity reduction for residual oil by ultrasonic. Ultrason. Sonochem. 41, 661–669.

Imoisili, P., Ukoba, K., Jen, T., 2020. Green Technology Extraction and Characterisation of Silica Nanoparticles from Palm Kernel Shell Ash via Sol-Gel. J. Mater. Res. Technol. 9 (1), 307–313.

Jafari, V., Allaverdi, A., Vafaei, M., 2014. Ultrasonic-Assisted Synthesis of Colloidal Nanosilica from Silica Fume: Effect of Sonication on the Properties of Product. Adv. Powder Technol. 25, 1571–1577.

Jani, Y., Hogland, W., 2017. Reduction-melting extraction of trace elements from hazardous waste glass from an old glasswork's dump in the South Eastern part of Sweden. Environ. Sci. Pollut. Res. 24, 26341–26349.

Jie, C.K., Jaafar, M.Z., Wan Sulaiman, W.R., 2019. Foam Stability Performance Enhanced with Rice Husk Ash Nanoparticles. Jurnal Teknologi (Sciences & Engineering) 81 (4), 97–196.

Kaya, A., Yukselen, Y., 2005. Zeta Potential of Clay Mineral and Quartz Contaminated by Heavy Metals. J. Can. Geotechnical 42, 1280–1289.

Kazemzadeh, Y., Sharifi, M., Riazi, M., Rezvani, H., Tabaei, M., 2018. Potential effects of metal oxide/SiO2 nanocomposites in EOR processes at different pressures. Colloids Surf., A 559, 372–384.

Kenes, K., Yerdos, O., Zulkhair, M., Yerlan, D., 2012. Study on the Effectiveness of Thermally Treated Rice Husks for Petroleum Adsorption. J. Non-Crystal Solids 358, 2964–2969.

Krishnarao, R.V., Godkhindi, M.M., 1992. Distribution of Silica in Rice Husk and Its effect on the Formation of Silicon Carbide. Ceram. Int. 18, 243–249.

Kumar, D., Ganat, T., Lashari, N., Ayoub, M., Kalam, S., Chandio, T., Negash, B.M., 2022. Experimental investigation of GO-HPAM and SiO2-HPAM composite for cEOR: Rheology, interfacial tension reduction, and wettability alteration. Colloids Surf., A 637, 128189.

Lee, L., 2013. Continuous granulation of pharmaceutical powder using a twin screw granulator. University of Birmingham. PhD Thesis.

Li, F., Jiang, X., Zuo, Q., Li, J., Ban, B., Chen, J., 2020. Purification Mechanism of Quartz Sand by Combination of Microwave Heating and Ultrasound Assisted Acid Leaching Treatment. Silicon. https://doi.org/10.1007/s12633-020-00457-7.

Li, X., Pu, C., Chen, X., Huang, F., Zheng, H., 2021. Study on frequency optimization and mechanism of ultrasonic waves assisting water flooding in low-permeability reservoirs. Ultrasonics – Sonochemistry 70, 105291.

Lin, J., Yen, T., 1993. An Upgrading Process through Cavitation and Surfactant. Energy Fuels 7, 111–118.

Lin, X., Sun, S., Wang, B., Zheng, B., Guo, Z., 2020. Structural and physicochemical properties of lotus seed starch nanoparticles prepared using ultrasonic-assisted enzymatic hydrolysis. Ultrason. Sonochem. 68, 105199.

Liu, G., Zhou, B., Du, A., Shen, A., Yu, Q., 2013. Effect of the thermal treatment on microstructure and physical properties of low-density and high transparency silica aerogels via acetonitrile supercritical drying. J. Porous Mater. 20, 1163–1170.

Loh, Z., Samanta, A.S., Heng, P., 2015. Overview of Milling Techniques for Improving the Solubility of Poorly-Water Soluble Drugs. Asian Journal of Pharmaceutical Science 10, 255–274.

Maghzi, A., Mohebbi, A., Kharrat, R., Ghazanfari, M.H., 2013. An Experimental Investigation of Silica Nanoparticles Effect on the Rheological Behaviour of Polyacrylamide Solution to Enhance Heavy Oil Recovery. Pet. Sci. Technol. 31, 500–508.

Marrow, A.W., Mukhametshina, A., Aleksandrov, D., Hasckir, B., 2014. Environmental Impact of Bitumen Extraction with Thermal Recovery. Paper SPE-170066-MS, presented at the SPE Heavy Oil Conference-Canada, Calgary, Alberta, Canada, June.

Mateus, L., Taborda, E.A., Moreno-Castilla, C., Lopez-Ramon, M. V., Franco, C.A., Cortes, F.B., 2021. Extra-Heavy Crude Oil Viscosity Reduction Using and Reusing Magnetic Copper Ferrite Nanospheres. Processes 9, 175.

Mohammadian, M., Junin, R., Rahmani, O., Idris, A., 2013. Effect of Sonication Radiation on Oil Recovery by Ultrasonic Waves Stimulated Water Flooding. Ultrasonics 53, 607–614.

Montes, D., Cortes, F., Franco, C., 2018. Reduction of heavy oil viscosity through ultrasound cavitation assisted by NiO nanocrystals-functionalized SiO2 nanoparticles. DYNA 85 (207), 153–160.

Mullakaev, M.S., Abramov, V.O., Abramova, A.V., 2017. Ultrasonic automated oil well complex and technology for enhancing marginal well productivity and heavy oil recovery. J. Petrol. Sci. Eng. 159, 1–7.

Nayak, P., Nandi, S., Datta, A.K., 2019. Comparative assessment of chemical treatments on extraction potential of commercial grade silica from rice husk. Engineering Reports doi.org/10.1002/eng2.12035.

Nezhad, S.S.K., Cheraghian, G., 2016. Mechanisms behind injecting the combination of nano-clay particles and polymer solution for enhanced oil recovery. Appl. Nanosci. 6, 923–931.

Olaya-Escobar, D., Quintana-Jimenez, L., Gonzalez-Jimenez, E., Olaya-Escobar, E., 2020. Ultrasound Applied in the Reduction of Viscosity of Heavy Crude Oil. Revista Facultad de Ingeniería 29 (54), e11528.

Onaja, E., Attan, N., Chandren, S., Razak, F.I.A., Keyon, A.S.A., Mahat, N.A., Wahab, R.A., 2017. Malaysian J. Fundamental Appl. Sci. 13 (4), 623–631.

Pineda-Vasquez, T., Casas-Botero, A., Ramírez-Carmona, M., Torres-Taborda, M., Soares, C., Hotza, D., 2014. Biogeneration of Silica Nanoparticles from Rice Husk Ash Using Fusarium oxysporum in Two Different Growth Media. Ind. Eng. Chem. Res. 53 (17), 6959–6965.

Reynolds, R., Markland, K., Rood, J., Leonard, E., Saunders, S., 2016. Manipulating Ligand-Nanoparticles Interaction and Catalytic Activity Through Organic-Aqueous Tunable Solvent Recovery. RSC Adv. 6, 78496.

Rezvani, H., Panahpoori, D., Riazi, M., Parsaei, R., Tabaei, M., Cortes, F.B., 2020. A novel foam formulation by Al_2O_3/SiO_2 nanoparticles for EOR applications: A mechanistic study. J. Mol. Liq. 304, 112730.

Rovani, S., Santos, J., Corio, P., Fungaro, D., 2018. Highly Pure Silica Nanoparticles with High Adsorption Capacity Obtained from Sugarcane Waste Ash. ACS Omega 3, 2618–2627.

Saboorian-Jooybari, H., Dejam, M., Chen, Z., 2016. Heavy Oil Polymer Flooding from Laboratory Core Floods to Pilot Test and Field Applications: Half-Century Studies. J. Petrol. Sci. Eng. 142, 85–100.

Sakthivel, S., Krishnan, V., Pitchumani, B., 2007. Influence of Suspension Stability on Wet Grinding for Production of Mineral Nanoparticles. Particuology 6, 120–124.

Sandri, G., Bonferoni, M.C., Rossi, S., Caramella, C.M., (2013) The Role of Particle Size in Drug Release and Absorption. In: Merkus H., Meesters G. (eds) Particulate Products. Particle Technology Series, 19. Springer, Cham. https://doi.org/10.1007/978-3-319-00714-4_11.

Sen, S., 2017. Grinding of magnetite using a waterjet driven cavitation cell. Powder Technol. 297, 34–43.

Singh, J., Kaur, L., McCarthy, O., 2007. Factors Influencing the Physio-Chemical, Morphological, Thermal, and Rheological Properties of Some Chemically modified Starches for Food Applications-A Review. Food Hydrocolloids 21, 1–22.

Soleimani, E., Mohammadi, M., 2018. Synthesis, characterization and properties of polystyrene/NiO nanocomposites. J. Mater. Sci.: Mater. Electron. 29, 9494–9508.

Sukmarani, G., Ledyastuti, M., 2019. The Properties of Microcellulose as Enhanced Oil Recovery Agent. J. Phys. Conf. Ser. 1245, 012041.

Sviridov, A., Tomarov, K., Fesenko, I., Xu, W., Andreev, V., Timoshenko, V., Lehto, V., 2019. Cavitation Induced by Janus-Like Mesoporous Silicon Nanoparticles Enhances Ultrasound Hyperthermia. Front. Chem., https://doi.org/10.3389/fchem.2019.00393.

Tettey, K., Lee, D., 2013. Effect of Thermal Treatment and Moisture Content on the Charge of Silica Particles in Non-Polar Media. Soft Matter 9, 7242.

Thompson, L., Doraiswamy, L., 1999. Sonochemistry: Science and Engineering. Ind. Eng. Chem. Res. 38, 1215–1249.

Wan, C., Wang, R., Zhou, W., Li, L., 2019. Experimental Study on Viscosity Reduction of Heavy Oil by Hydrogen Donors Using Cavitating Jet. RSC Adv. 9, 2509.

Wang, F., Zhou, L., Zhou, J., Gu, X., Feng, Y., 2010. Characterization of anticancer hypocrellin A encapsulated with silica nanoparticles. J. Therm. Anal. Calorim. 102, 69–74.

Wang, J., Liu, J., Zhang, L., Li, Z., 2014. Aquathermolysis of Heavy Crude Oil with Amphiphilic Nickel and Iron Catalysts. Energy Fuels 28 (12), 7440–7447.

Wang, H., Mustaffa, A., Phan, A., Zivkovic, V., Reay, D., Law, R., Boodhoo, K., 2017. Review of Process Intensification Applied to Solid Handling. Chem. Eng. Process. Process Intensif. 118, 78–107.

Yakasai, F., Jaafar, M.J., Bandyopadhyay, S., Agi, A., 2021. Current developments and future outlook in nanofluid flooding: A comprehensive review of various parameters influencing oil recovery mechanisms. J. Ind. Eng. Chem. 93, 138–162.

Zhang, J., Yang, Y., Chen, Z., Yan, Y., Zhao, J., Li, J., 2018. In Situ synthesis of SiC-graphene core-shell nanoparticles using wet ball milling. Ceram. Int. 14 (7), 8283–8289.